GEOTHERMAL HEAT FLOW ANALYSIS OVER

THE UPPER SOKOTO BASIN, NIGERIA

USING AEROMAGNETIC DATA.

BY

ONYEDIBE, Elochukwu Charles

M.TECH/S.S.S.E/2009/2284

DEPARTMENT OF PHYSICS,

FEDERAL UNIVERSITY OF TECHNOLOGY

MINNA.

OCTOBER, 2012

ABSTRACT

Geothermal Heat Flow Analysis over the Upper Sokoto Basin Nigeria, using Aeromagnetic Data was carried out to determine the geothermal heat flow in the area. The study area extends from latitude 12.50°N to 13.50°N and Longitude 4.00°E to 6.00°E. Polynomial fitting method was applied in the regional – residual separation from the digitised data. The observed magnetic residual anomalies map was Fourier transformed after dividing the area into 24 overlapping sections for spectral analysis and interpretation. The Spectral plot reveals two layers of magnetic sources. The Basement depth (D_2) varies from 0.505 km to 1.77 km with an average value of 1.240 km, while the Centroid depth (D_3) varies from 3.495 km to 8.110 km with an average of 4.763 km. Thus D_3 values were used to obtain an approximate contour map of the basement surface in the basin. The curie - point depth estimated from the spectral analysis varies from 5.720 to 14.840 km with average of 8.285 km. Contour map of the curie- point depth and its corresponding 3-D Model were generated. The calculated geothermal gradient and heat flow for the study area varies between 20.216 to 52.447 °C/km and 36.388 to 94.405 mW/m^2 respectively. The general trend shows that the area with the highest heat flow value (94.405 mW/m^2) found in the north-eastern region of the study area correspond to the area with the highest geothermal gradient and vice-versa, also with shallow curie-point depth. This area is likely a geothermal source potential zone.

TABLE OF CONTENTS

CHAPTER ONE

CHAPTER FOUR

CHAPTER FIVE

LIST OF TABLES

LIST OF FIGURES

ABBREVIATIONS

N	North
S	South
W	West
m	meter
^{o}C	Degree Celsius
D_2	Basement depth
D_3	Centroid Depth
$^{o}0$	Degree
km	kilometer
NE	Northeast
NW	Northwest
SE	Southeast
^{o}N	Degree North
^{o}E	Degree East
S/no	Serial Number
Log	Logarithm
mW/m^2	mill weber per meter square
$Wm^{-1o}C^{-1}$	weber per meter degree Celsius
%	Percentage
g/cm^3	gram per centimeter cube

APPENDIX A

Apendix A   **Page**

CHAPTER ONE

1.0   INTRODUCTION

1.1   Geophysics

Geophysics is a branch of science that applies physical principles to the study of the earth. Geophysicists examine physical phenomena and their relationships within the earth; such phenomena include the earth's magnetic field, heat flow, the propagation of seismic (earthquake) waves, and the force of gravity. The scope of geophysics also broadly includes outer-space phenomena that influence the earth, the effects of the sun on the earth's magnetic field; and manifestations of cosmic radiation and the solar wind. (Finkl, 2000).

The scientific record of mining and exploration geophysics began with the publication of the famous Treaties *De Re* Metalica by Georgius Agricola in 1965 (Telford, 1976). The initial step in the application of geophysics to the search for minerals probably was taken in 1843, when Von Wrede pointed out that the magnetic theodolite used by Lamout to measure variations in the earth's magnetic field might also be engaged to discover magnetic ore bodies (Telford, 1976). The constant increase in the demand for metals of all categories and the massive increase in the use of oil and natural gas during the previous years have led to the expansion of many geophysical techniques with increasing sensitivity for the discovery and mapping of hidden deposits and structures. Improvements have been particularly rapid during the previous decade or so because of the expansion of new electronic devices for field equipment and widespread application of the digital computer in the interpretation of geophysical data (Telford, 1976).

Geophysical exploration, commonly called applied geophysics or geophysical prospecting, is conducted to locate economically significant accumulations of oil, natural gas, groundwater

and other minerals. Geophysical investigations are also employed with engineering objectives in mind, such as predicting the behaviour of earth materials in relation to foundations for roads, railways, buildings, tunnels, and nuclear power plants. Surveys are generally identified by the property being measured namely: electrical, gravity, magnetic, seismic, thermal, or radioactive properties. Electrical and electromagnetic surveys map variations in the conductivity or capacitance of rocks measured by special tools lowered into holes drilled for oil and gas, conductivity variations provide geophysicists with clues from which they can judge the hydrocarbon-bearing potential of rock strata. Direct and alternating electrical currents are measured in ground surveys, but the lower radio frequencies are used both in ground and in airborne electromagnetic surveys. Gravity surveys measure density variations in local rock masses, used mainly in petroleum exploration, these surveys are based on use of a device called a gravimeter, gravity surveys are made on land, at sea, and down boreholes.

Geothermal surveys concentrate on temperature variations and the generation, conduction, and loss of heat within the earth. Geothermometry is also important to volcanologic studies as well as to locating geothermal energy resources (Finkl, 2000).

The choice of techniques applied to locate a certain mineral depends upon the nature of the mineral and of the surrounded rocks. Occasionally a method may give a straight signal of the occurrence of the mineral being sought, for instance, the magnetic method when used to find magnetic ore of iron or nickel; at other time the method may only indicate whether or not the condition are encouraging to the occurrence of the mineral sought for example the magnetic method which is frequently used in petroleum exploration as an investigation tool to discover the depth to the igneous basement rocks and so examine where the sediments are thick enough to permit exploration for petroleum (Finkl, 2000).

1.2   Aeromagnetic Survey:

Aeromagnetic survey is a common type of geophysical survey carried out using a magnetometer aboard or towed behind an aircraft. The principle is similar to a magnetic survey carried out with a hand-held magnetometer, but allows much larger areas of the Earth's surface to be covered quickly for regional reconnaissance. The aircraft typically flies in a grid-like pattern with height and line spacing determining the resolution of the data and cost of the survey per unit area (Burger *et al,* 2006).

As the aircraft flies, the magnetometer records tiny variations in the intensity of the ambient magnetic field due to the temporal effects of the constantly varying solar wind and spatial variations in the Earth's magnetic field, the latter being due both to the regional magnetic field, and the local effect of magnetic minerals in the Earth's crust. By subtracting the solar and regional effects, the resulting aeromagnetic map shows the spatial distribution and relative abundance of magnetic minerals (most commonly the iron oxide mineral magnetite) in the upper levels of the crust, because different rock types differ in their content of magnetic minerals, the magnetic map allows a visualization of the geological structure of the upper crust in the subsurface, particularly the spatial geometry of bodies of rock and the presence of faults and folds. This is particularly useful where bedrock is obscured by surface sand, soil or water. Aeromagnetic data was once presented as contour plots, but now is more commonly expressed as coloured and shaded computer generated pseudo-topography images. The apparent hills, ridges and valleys are referred to as aeromagnetic anomalies. A geophysicist can use mathematical modelling to infer the shape, depth and properties of the rock bodies responsible for the anomalies (Burger *et al,* 2006).

Aeromagnetic surveys are widely used to aid in the production of geological maps and are also commonly used during mineral exploration. Some mineral deposits are associated with an increase in the abundance of magnetic minerals, and occasionally the sought after commodity may itself be magnetic (e.g. iron ore deposits), but often the elucidation of the subsurface structure of the upper crust is the most valuable contribution of the aeromagnetic data.

Aeromagnetic surveys are now used to perform reconnaissance mapping of unexploded ordnance (UXO). The aircraft is typically a helicopter, as the sensors must be close to the ground (relative to mineral exploration) to be effective. Electromagnetic methods are also used for this purpose. (Burger *et al*, 2006)

Aeromagnetic surveys are extensively used as investigation tools and there has been an increasing acknowledgment of their value for evaluating potential areas by virtue of the unique information they provide. Sharma (1987) outlined the roles of aeromagnetic survey as follows:

1. Explanation of volcano-sedimentary belts under sand or other recent cover, or in strongly transformed terrains when recent lithologies are otherwise unrecognisable.

2. Recognition and interpretation of faulting shearing and fracturing not only as potential host for a variety of minerals, but also an indirect guide to epigenetic stress related mineralisation in the surrounding rocks.

3. Identification and delineation of post tectonic intrusion, typical of such targets are zoned syenite or carbonatite, complexes, kinerlites, tin-bearing granites and mafic intrusions.

4. Direct detection of deposits of certain iron ores.

5. In prospecting for oil, aeromagnetic data can give information from which one can determine depths to basement rocks and thus locate and define the extent of sedimentary basins. Sedimentary rocks however ectent such a small magnetic intensity in measurable at the surface result from topographic or lithologic changes associated with basement or from igneous intrusion (Dobrin, 1976).

1.3 Earth Crust

The crust is the outermost solid shell of a rocky planet or natural satellite, which is chemically separate from the underlying mantle. The crusts of Earth, Moon, Mercury, Venus, Mars and other terrestrial bodies have been generated largely by igneous rock. Below is the Earth cutaway from core to exosphere.
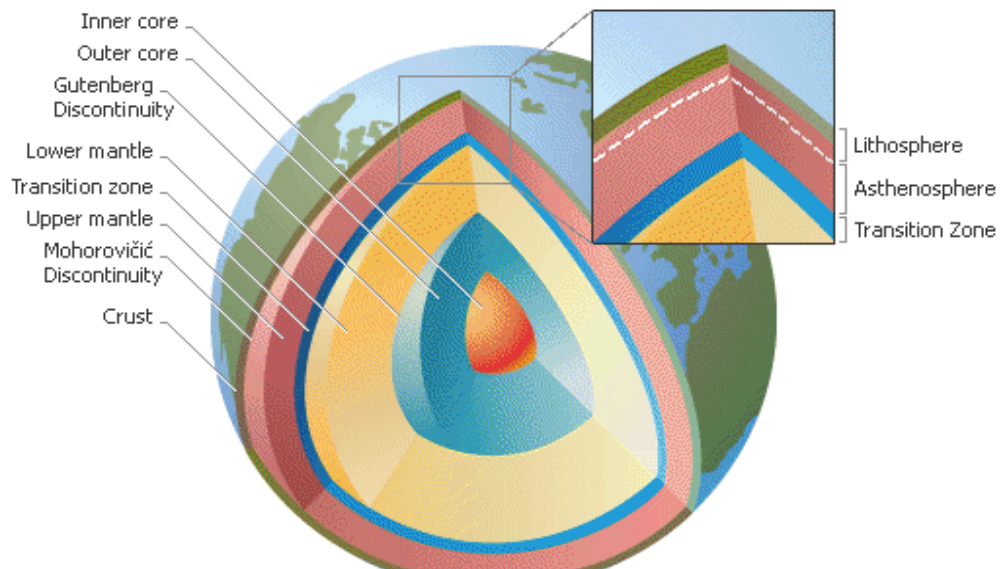

Figure 1.1 Earth Cutaway from core to exosphere (Source: Microsoft Encarta)

The crust of the Earth is composed of a great variety of igneous, metamorphic, and sedimentary rocks. The crust is underlain by the mantle. The upper part of the mantle is composed mostly of peridotite, a rock denser than rocks common in the overlying crust. The boundary between the crust and mantle is conventionally placed at the Mohorovičić discontinuity, a boundary defined by a contrast in seismic velocity (Patchett and Samson, 2003). Earth's crust occupies less than 1% of Earth's volume.

The oceanic crust of the sheet is different from its continental crust. The oceanic crust is 5 km (3 mi) to 10 km (6 mi) (Patchett and Samson, 2003) thick and is composed primarily of basalt, diabase, and gabbro. The continental crust is typically from 30 km (20 mi) to 50 km (30 mi) thick, and is mostly composed of slightly less dense rocks than those of the oceanic crust. Some of these less dense rocks, such as granite, are common in the continental crust but rare to absent in the oceanic crust. Both the continental and oceanic crust "float" on the mantle, because the continental crust is thicker, it extends both above and below the oceanic crust, much like a large iceberg floating next to smaller one. (The slightly lighter density of felsic continental rock compared to basaltic ocean rock also contributes to the higher relative elevation of the top of the continental crust.) Because the top of the continental crust is above that of the oceanic, water runs off the continents and collects above the oceanic crust. The continental crust and the oceanic crust are sometimes called sial and sima respectively. Due to the change in velocity of seismic waves it is believed that on continents at a certain depth sial becomes close in its physical properties to sima and the dividing line is called The Conrad Discontinuity. The temperature of the crust increases with depth, reaching values typically in the range from about 200 °C (Patchett and Samson, 2003) (392 °F) to 400 °C (752°F) at the boundary with the underlying mantle. The crust and underlying relatively rigid uppermost

mantle make up the lithosphere. Because of convection in the underlying plastic (although non-molten) upper mantle and asthenosphere, the lithosphere is broken into tectonic plates that move. The temperature increases by as much as 30°C (about 50°F) for every kilometre locally in the upper part of the crust, but the geothermal gradient is smaller in deeper crust
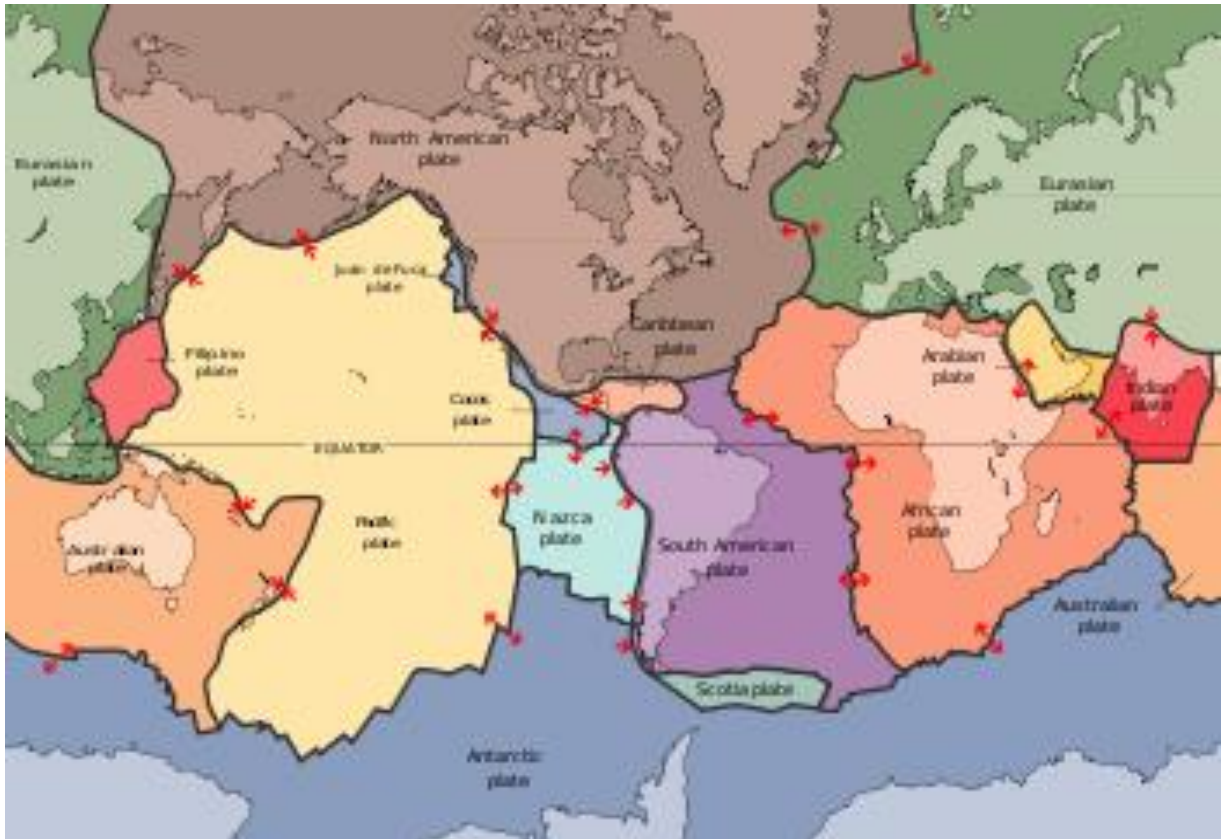
**Figure 1.2   Plates in the crust of the earth, according to the plate tectonics
(Source: Microsoft Encarta 2009)**

Theory aggregate of planetesimals into its core, mantle and crust within about 100 million years of the formation of the planet, 4.6 billion years ago. The primordial crust was very thin, and was probably recycled by much more vigorous plate tectonics and destroyed by significant asteroid impacts, which were much more common in the early stages of the solar system.

The Earth has probably always had some form of basaltic crust, but the age of the oldest oceanic crust today is only about 200 million years. In contrast, the bulk of the continental crust is much older. The oldest continental crustal rocks on Earth have ages in the range from about 3.7 to 4.28 billion years and have been found in the Narryer Gneiss Terrane in Western Australia, in the Acasta Gneiss in the Northwest Territories on the Canadian Shield, and on other cratonic regions such as those on the Fennoscandian Shield. A few zircons with ages as great as 4.3 billion years have been found in the Narryer Gneiss Terrane.

The average age of the current Earth's continental crust has been estimated to be about 2.0 billion years (Patchett and Samson, 2003). Most crustal rocks formed before 2.5 billion years ago are located in cratons. Such old continental crust and the underlying mantle asthenosphere are less dense than elsewhere in the earth and so are not readily destroyed by subduction. Formation of new continental crust is linked to periods of intense orogeny or mountain building; these periods coincide with the formation of the supercontinents such as Rodinia, Pangaea and Gondwana. The crust forms in part by aggregation of island arcs including granite and metamorphic fold belts, and it is preserved in part by depletion of the underlying mantle to form buoyant lithospheric mantle.

1.3.1 Continental Crust
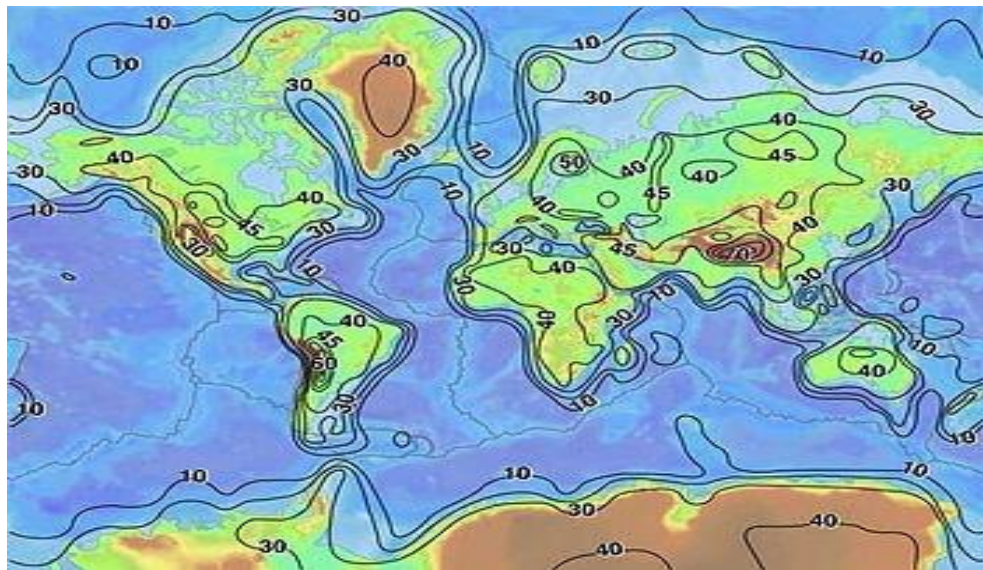
Figure 1.3   The thickness of the Earth's crust (Source: Microsoft Encarta 2009)

The continental crust is the layer of igneous, sedimentary, and metamorphic rocks which form the continents and the areas of shallow seabed close to their shores, known as continental shelves. This layer is sometimes called *sial* due to more felsic, or granitic, bulk composition, which lies in contrast to the oceanic crust, called *sima* due to its mafic, or basaltic rock. (Based on the change in velocity of seismic waves, it is believed that at a certain depth *sial* becomes close in its physical properties to *sima*. This line is called the Conrad discontinuity.)

Consisting mostly of granitic rock, continental crust has a density of about 2.7 g/cm^3 and is less dense than the material of the Earth's mantle, which consists of mafic rock. Continental crust is also less dense than oceanic crust (density of about 3.3 g/cm^3), though it is considerably thicker; mostly 25 to 70 km versus the average oceanic thickness of around 7–10 km. About 40% of the Earth's surface is now underlain by continental crust. Continental crust makes up about 70% of the volume of Earth's crust (Armstrong, 1991).

1.4   Geothermal

Geothermal Energy, energy contained in intense heat that continually flows outward from deep within Earth, this heat originates primarily in the core. Some heat is generated in the crust, the planet's outer layer, by the decay of radioactive elements that are in all rocks. The crust, which is about 5 to 75 km (about 3 to 47 mi) thick, insulates the surface from the hot interior, which at the core may reach temperatures from 4000° to 7000° C (7200° to 12,600° F). Where the heat is concentrated near the surface, it can be used as a source of energy. (Nemzer, *et al*., 2009)

1.4.1   Geothermal Geology

The distance from Earth's surface to its centre is about 6,500 km (about 4,000 mi). From Earth's surface down through the crust, the normal temperature gradient (the increase of temperature with increase of depth) is 10° to 30° C per km (29° to 8 7°F per mi). Underlying the crust is the mantle, which is made of partially molten rock. Temperatures in the mantle may reach 3700° C (6700° F). The convective (circulating) motion of this mantle rock drives plate tectonics—the 'drift' of Earth's crustal plates that occurs at a rate of 1 to 5 cm (0.4 to 2 in) per year. Where plates spread apart, molten rock (magma) rises up into the rift (opening), solidifying to form new crust. Where plates collide, one plate is generally forced (sub ducted) beneath the other. As the sub ducted plate slides slowly downward into the mantle's ever-increasing heat, it melts forming new magma. Plumes of this magma can rise and intrude into the crust, bringing vast quantities of heat relatively close to the surface. If the magma reaches the surface it forms volcanoes, but most of the molten rock stays underground, creating huge subterranean regions of hot rock.
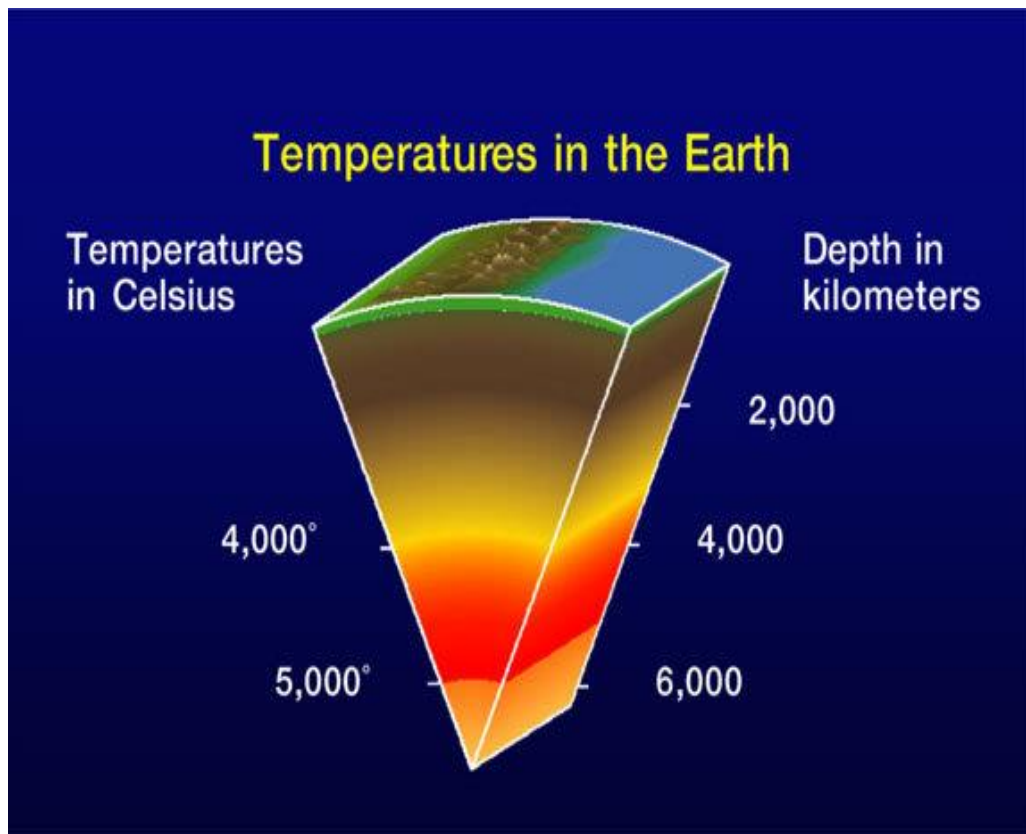
Figure 1.4   Temperatures in the Earth (Source: Microsoft Encarta 2009)

1.4.2 Geothermal Reservoirs

In certain areas, water seeping down through cracks and fissures in the crust comes in contact with this hot rock and is heated to high temperatures. Some of this heated water circulates back to the surface and appears as hot springs and geysers. However, the rising hot water may remain underground in areas of permeable hot rock, forming geothermal reservoirs. Geothermal reservoirs, which may reach temperatures of more than 350 °C (700 °F), can provide a powerful source of energy.

Geysers are caused when underground chambers of water are heated to the boiling point by volcanic rock. When heat causes the water to boil, pressure forces a superheated column of steam and water to the surface. Because most geothermal reservoirs are capped by overlying rock, the heated water cannot escape, remaining underground instead. If a geothermal reservoir is sufficiently close to the surface, the heated water can be piped to the surface and used to produce energy
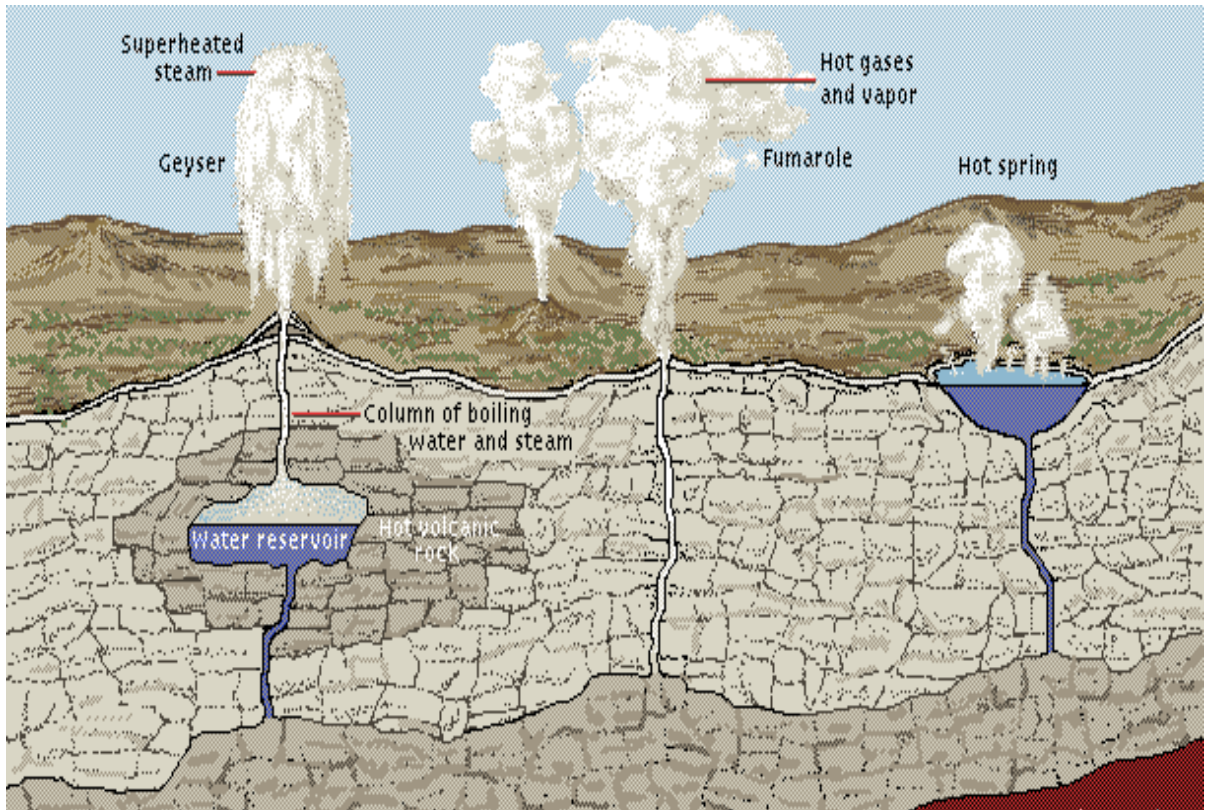
Figure 1.5 Formation of Geyser (Source: Microsoft Encarta 2009)

1.5   Source of Data for the Present Study

The study area covers the upper Sokoto Basin in the north-western part of Nigeria. The Basin consists predominantly of a gentle undulating plain, underlain by metamorphic rocks. The study area is covered by eight (8) digitised aeromagnetic maps. The digitised aeromagnetic maps were numbered 8, 9, 10, 11, 27, 28, 29 and 30 and the names of the places each map covers are also written on them for easy reference. The maps were produced by Nigerian Geological Survey Agency (NGSA) between 1974 and 1980.

1.6   Aim and Objectives of the Study Area

The main aim of this study area is to use the aeromagnetic maps of the area for depth computation, and applying spectral method for the production of geothermal facts of the study area. The depths are used to map the surface plot of the areas according to depths computed for the area. This map of crustal thickness and thermal data will furthermore provide insight on the crustal resolution as it relates to volcanoes, tectonic and fault system in the study area. Thus, these pieces of information on crustal thickness and temperature can contribute to the improvement of global crustal thickness and heat flow map respectively. This research method corresponded with the Spectral Analysis of the Magnetic Residual Anomalies over Sokoto basin carried out by Shehu *et al*., (2004).

1.7   The Methodology of the Study

The Procedures involved in this research project are outlined below:

i.   Digitised aeromagnetic maps covering the upper part of the Sokoto basin and the surrounding rocks were obtained.

ii.   All the digitised aeromagnetic maps were combined into a single supper map. This supper map or composite aeromagnetic map of the study area formed the basis for further analysis and interpretation.

iii.   The regional magnetic field map for the area was determined by fitting order polynomial field (because of simple geology and limited spatial extent of the study area) (Spector and Grant 1970) to the total field data using the least square method. The residual magnetic field will then be extracted by subtracting the regional field from the total field.

iv.   Estimations of the depth to layers of magnetisation in the upper Sokoto basin were carried out using spectral analysis of the residual magnetic field. Contour and surface maps of the second layers depths will produced and qualitatively discussed.

v.   The result generated from spectral techniques data set and maps provide a guide to regional crustal thickness reconnaissance studies. It has been understood that average depth of an ensemble magnetic source can be calculated using spectral analysis (Spector and Grant, 1970; Shuey *et al.,* 1977). Therefore estimate of curie-point isotherm depth (Crustal depth) use this depth and thickness information to predict if the area of study is viable for geothermal energy source. The Curie-point at which dormant rocks loosed their ferromagnetic properties provides a link between crustal depth models and models based on the analysis of magnetic

sources. The Curie isotherm may be analysed to produce geothermal gradient and heat flow

data, which are major observable parameters for geothermal and mineral exploration.

CHAPTER TWO

2.0   **Literature Review**

2.1   Geology of the Study Area

The upper Sokoto Basin is situated in the North-western part of Nigeria and it is bounded by latitude 12°50N and 13°50N and longitudes 4°00E and 6°00E. This is sedimentary basin with gentle undulating plain varying from 250 to 400 meters above sea level. (In geophysics, a region in which the Earth's surface has subsided and has been covered by sediments. One mechanism for subsidence is thermal subsidence: the lithosphere cools and thickens, and due to the increased density of the cooler rocks the lithosphere sinks. A typical thickness of a sedimentary basin is a few kilometres but some basins have a thickness of 10 km or more. Subsidence is often impeded by the rigidity of the elastic lithosphere and the resulting flexure of the lithosphere results in near circular or linear basins with a radius or width of about 200 km). The basin form the south-eastern sector of the large, nearly circular sedimentary basin, generally referred to as the "Iullemmeden Basin" of West African, Figure 2.0. The term "Iullemmeden Basin" was first proposed by Raider in 1931, to define the sedimentary basin which extends from Mali and the western boundary of the Republic of Niger through northern Benin Republic and north western Nigeria into Eastern Niger and covers an area of about 700,000 square kilometres (Kogbe, 1979). The rock units are predominantly clay alternating with gritty sand unit; they are ill-sorted, poorly consolidated with gravel overlying the pre-Cambrian basement unconformable.

Figure 2.0   GEOLOGICAL MAP OF SOKOTO BASIN
(Source: Nigeria Geological Survey Agency NGSA.)

Table 2.1: Geological Sequence of the Sokoto Basin (Kogbe, 1979)

AGE	FORMATION	GROUP	ENVIRONMENT
Quaternary	Sandy drifts, laterites	-----	Continental
Eocene	Gwandu-Formation	"Continental-Terminal"	Continental
	Unconformity		
Late–Pala Eocene	Primary Oolitic Iron stone. Gamba Formation Kalambaina formation	Sokoto Group	Marine
	Unconformity		
Maastrichtian	Wurno Formation Dukamaje formation Taloka Formation	Rima Group	Brackish Water With marine Intercalation
	Unconformity		
Late Jurassic to earliest Cretaceous	IIIo and Gundumi Formation	Continental intercalaire	Continental
	Major Unconformity		
Precambrian	Basement Complex		
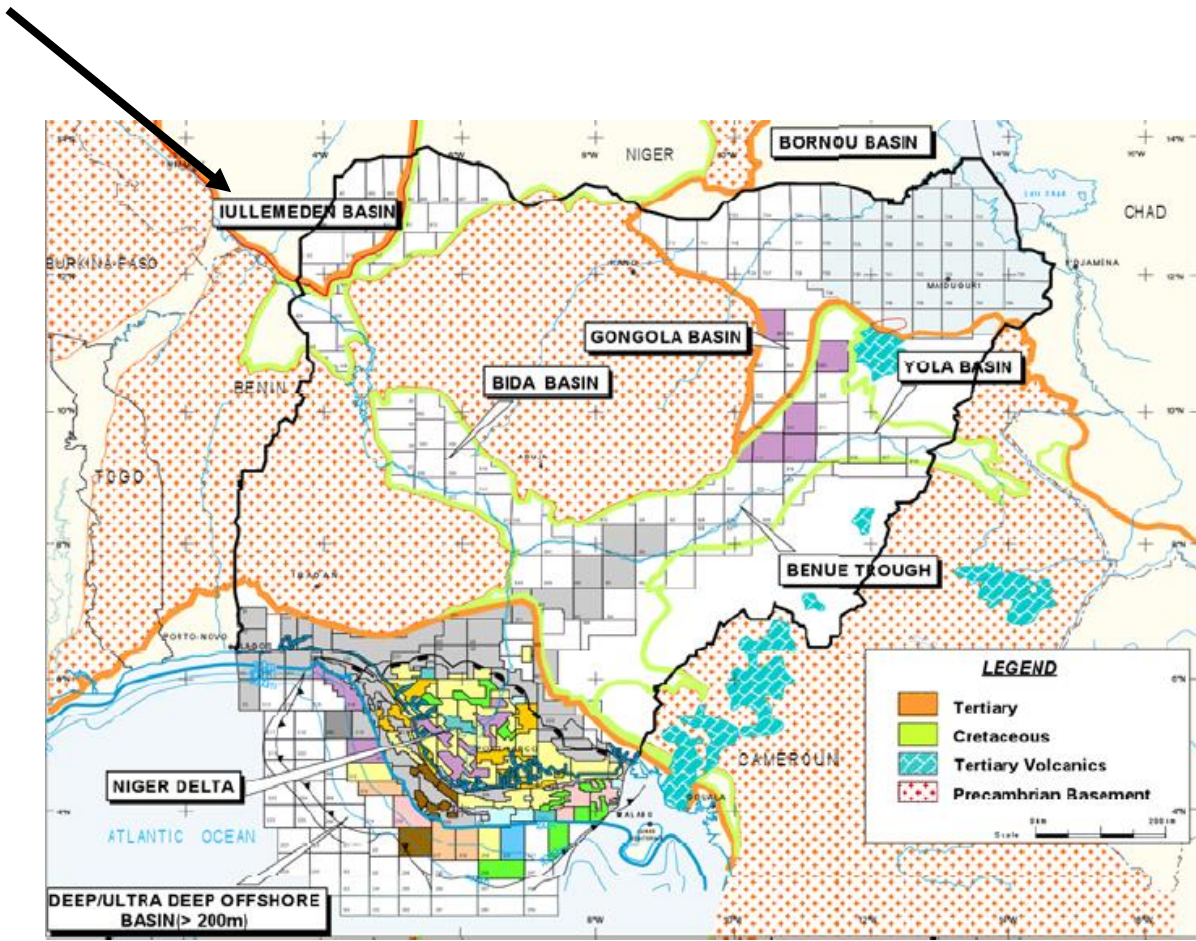
Figure 2.1: **Simplified Geological Map of the Study Area**
 (Source: www.google .com)

The upper Sokoto basin is dominated by sedimentary rocks which are always noticed in sedimentary basin, which Sokoto basin is an example.

The upper Sokoto basin is characterised by heavy sand deposit which later in its developmental stages resulted in sand formation. Generally, it is often called Sokoto Sand Formation. The Sand Formation usually occurred in layers, the young sand deposit rests directly on the old one horizontally with clay layers alternating with gritty sand units and reddish- brown in colour if viewed through soil profile. The best exposures of the Sokoto basin occur in the steep slope on the western side of the valley of the Gublin Sokoto. The upper strata are coarse white, friable false-bedded grits. The lower strata of the division are

intoned false-bedded grits studding with small quartz pebbles and clay nodules. The following sedimentary structures can be observed in well exposed outcrops: Rhythmic bedding (cyclothems), cross beds, wavy beds, flasser bedding, Ripple marks, mud cracks, clay galls and primary bedding (Kogbe, 1979).

2.1 Review of Previous Geophysical Studies in the Area.

Geological work in the Sokoto basin dated back to late 1800's, most of the published materials from this work relate to general geologic description of fossil localities. The Geological Survey of Nigeria in 1930 carried out electrical, resistivity, electromagnetic and seismic refraction surveys in different parts of the basin. The surveys were aimed at studying the aquifers of the basin with a view to selecting favourable sites for ground water boreholes. The results of some of these surveys have been published in form of bulletins or as special publications (Raeburn and Tattan, 1930). Unfortunately only one or two of the numerous boreholes scattered over the basin is/are known to have reached the basement and as such depth to basement estimates have been by extrapolations.

Between 1974 and 1980 the Geological Survey of Nigeria (GSN) carried out aeromagnetic mapping of the Sokoto basin, and the result of the survey has been published as contour map on a scale of 1:100,000. Sokoto basin has not attracted much geophysical attention apparently because of the belief that no proven hydrocarbon accumulation or mineral resource potentials have been indicated in these areas.

Umego (1990) carried out a gravity survey over part of the basin. This was complemented by the analysis of the aeromagnetic data over the basin area. He compared the result obtained from gravity and magnetic analysis and noted a significant difference in the depth to basement estimates from both methods. The magnetic depth to basement estimates through gravity

method was 1.0 km at one of the depressions. While the magnetic methods yielded a value of 1.4 km at the same location. At another location comparison showed estimate of 0.8 km and 1.6 km for the gravity and magnetic methods respectively, because of this significant differences, he suggested that boreholes and seismic information would considerably assist in constraining the model.

Between 1964 and 1967 United Nations project involving the use of aeromagnetic, aero electromagnetic, electrical and magnetic methods was carried out in the area indicated the need for more detailed study of the basin coupled with advancement in science and technology so as to ascertain its structure and depth to the basement underlying the sedimentary basin.

Shehu *et al.,* (2004) Carried out a research in sokoto basin on the Spectral Analysis of the Magnetic Residual anomalies over sokoto basin, in his research he determined the average depth to the magnetic basement rock by using spectral analysis of the residual magnetic field values over the study area, he observed magnetic residual anomalies by dividing the study area into 60 sections each of 14 x 14 overlapping grid blocks for the purpose of analysis and interpretation.

The spectral plots in the research reveals two clear layers of magnetic sources, the first layer depth vary from 0.10 km to 0.61 km with an average of 0.367 km while the second layer which represent depths to the basement magnetic rock vary from 0.34 km to 1.99 km an average value of 1.386 km. he concluded that the second layer average depth is rather small to allow for the accumulation of hydrocarbon.

Ewa and Krzysztof, (2010) carried out research on Geothermal Exploration in Nigeria. The investigation of sedimentary province carried out within the part of Sokoto basin in the research shows that the temperature data from water well in Sokoto basin is 0.9 to 7.6^{o}c/100m, thus the geothermal anomalies indicates that the zone of highest gradient in Sokoto basin is elongated in SW-NE direction, parallel to general strike of major sedimentary formations which are very thin in that area (about 200m). They suggest that a significant source of geothermal heat is located below sedimentary complex in Precambrian basement and perhaps is related to some deep tectonic active structure.

They concluded that geothermal analysis based on geothermal gradients indicated area of higher than average gradient value and geothermal anomalies within sedimentary basins. It is possible to conduct more precise study of geothermal gradients if temperature data from oil and gas exploration wells from Benue trough, Chad and Sokoto basin are available.

2.2   Tectonic Evolution of Sokoto Basin

According to Bertrand – Sarfati *et al.,* (1977), the Iullemmeden basin in its totality is a cratonic basin created by tectonic epeirogenic movements within cratonic rocks. These movements became evident from the beginning of the Palaeozoic and continued until the upper cretaceous when the opening of the Goa Trench was achieved. They become progressively younger as one moves towards the SW from the North.

Kogbe (1979) observed that the Iullemmenden basin in which Sokoto basin is a part of cratonic basin created by tectonic epeirogenic movements. One can rightly conclude based on the work of Bertrand – Sarfati *et al.,* (1977) and Kogbe (1979) as follows:

(a)   That Sokoto basin, being a sedimentary basin, probably originated from the tectonic epeirogenic movements within cratonic rocks in Nigeria.

(b)   The Sokoto basin in south-eastern sector of Iullemmedian basin belongs to the class of sedimentary basins related to continental plate divergence in West Africa. They are typically broad cratonic epierogenic basin.

2.3 Economic Geology of the Sokoto Basin

Sokoto sand formation, which is an example of sedimentary rock are of great importance to the people of the immediate environment especially in the areas of Agriculture practices and secondly Brick makes uses it as a raw materials.

The most important economic minerals in the Sokoto Basin are the industrial minerals consisting of clays, ironstones and laterites, gypsum, limestone, gravel and lignite.

Clay deposits are abundant in Sokoto basin over large area, the composition of the clay is that of relatively pure Kaolin with a small excess of alumina and less than 1% iron oxides. Clays also occur abundantly in the Gwandu formation, as in kwondomo village about ten kilometres south of llela on the Sokoto road. These Gwandu formation clays are white in colour and often occur as nodules or roundish balls indicating some turbulent localities in the depositional environment. The clay that outcrops at several localities forms a bed of over 2 meters thick, overlain by a thin layer of ferruginised sandstone; the main deposits are present exploited for local building. The clay is silt white or mottled as in the basal part and coated with iron oxide films along joints and fractures.

Gypsum, which is an essential ingredient in the manufacture of cement, is also in abundance. Its presence was first reported by (Falconer, 1911). Two horizons of gysiferous shales are known in the sokoto basin: the Dukamaje Formation and Dange Formation.

The establishment of the cement factory in Sokoto has produced a market for local gypsum which is extracted in the form of local pitting by the inhabitants of the Rima valley, the gypsum of the shale horizon are present in crystals and stripes of the selenite variety averaging three to four centimetre in length, it occupies fractures bedding planes, joints and

cavities and are practically always associated with iron oxides. In the thinner fractures the walls are covered by a layer of gypsum while the core is composed of limonite in the large fractures. Iron oxide can be absent and in the cavities gypsum can appear in well-developed crystals with the characteristic twinning structure.

Iron as a solid mineral also abounds in sediments and alluvial deposits in Sokoto basin and heaps of iron slag are found in various parts of the basin. This may facilitate the establishment of smelting industries. Limestone is found in Dukamaje, Dange, and Kalambaina formations, limestone is at present exploited by the sokoto cement company of Northern Nigeria. The main source of water within Sokoto basin is the rivers, lakes and wells. Villages along the banks of the main rivers depend on the rivers for their entire water supply. A large proportion of the wells sunk are dry, due to either a disregard in the siting, for the local geology, or to misuse by the local inhabitants which results in stagnation. The iron stone is porous and yields its water freely, often supplying water to large herds of Fulani livestock in addition to the local inhabitants. Though the report of the study for ground water development in Sokoto by Japan International Co-operation Agency (JICA 1990) shows that sedimentary rock of the basin composed of sandstone, limestone and clay of cretaceous to the tertiary ages; forms a multi-layer ground water basin with pumping rate of 300 L/min at a well with 100 - 150m depth and 150 mm in diameter. The alluvia in fadama also contain unconfirmed groundwater. The Sokoto basin in Nigeria, like sedimentary basins in other parts of the worlds, provides possible source rocks, reservoir beds, and the structural environment required for the formation of petroleum. This accounts for its possible economic potential and the present geophysical surveys for the primary purpose of calculating the thickness of the sedimentary section.

CHAPTER 3

3.0 Materials and Methods

3.1 Data Collection and Merging

The study area, upper Sokoto is covered by eight (8) aeromagnetic maps. The maps were numbered 8, 9, 10, 11, 27, 28, 29 and 30 and the names of the places each map covers were also written on them for easy reference, the maps were obtained from Nigeria Geological Survey Agency (NGSA) and digitised.

The next step was to produce a unified aeromagnetic map of the study area; this was done on a spread sheet format, each coding sheet contains 28 by 28 coding sheets. Each coding sheet contains name of the town overflown, the map number and the boundary longitudes and latitudes. An acquired computer program was used to read in and reproduce the data as they are contained in each coding sheet. To ensure that no mistake was made during imputation into the computer, the output data was compared with the input data. The output data file contains magnetic values stating longitude and latitude of each map, this data file therefore was used as the input file for another program that would pick all the data point row by row, calculate their latitudes and longitude and produce the results in 3 columns (x, y, z), where x, y and z represent longitude, latitude and the magnetic values for the coordinates respectively. The three dimensional co-ordinate from x, y, z is the form that is acceptable to a contouring package "SURFER". Surfer is a menu driven interactive computer programme which places each magnetic data points according to their latitude and longitude bearing and thereafter produces a contour map for each of the eight aeromagnetic maps. The reason behind this contour map is to pictorially examine the contours and ensure that they correspond with those of its equivalent aeromagnetic map that was digitised.

The interpolated data recorded on the coding sheets for each map were merged together column to column and row to row as contained in Figure 3.1 to produce a unified dataset which in turn will be used to generate the combine aeromagnetic map (unified map). The problem of boundary edge effect was solved by adding all magnetic values with the same co-ordinate and then averaged so that there would not be rows and columns of magnetic points with the same coordinates.

Figure 3.1 below represents a rectangular outline of the Sokoto basin; each number in the figure represents a topographic map sheet measuring 30' by 30' on the sexagesimal scale and contains 28 by 28 (784) digitised magnetic values.

8	9	10	11
Sakkwabe	Binji	Sokoto	Rabah
27	28	29	30
Lema	Argungu	Dange	Gandi

Figure 3.1 - Study Area of 8 Aeromagnetic Maps.

At the boundary between two maps, for example map 8 and 9 have the same coordinates (latitude and longitude) as the field values at corresponding grid points of the first column of map 9. This also occurs between maps 9 and 10 and maps 10 and 11. Magnetic values at the edge in column forming 109 columns.

Also at the boundary between map 8 and 27 the magnetic field values at the last row of map 8 have the same coordinates as in the field values in the first row of map 27, this also occur

between 9 and 28, 10 and 29, 11 and 30, the points of the same coordinates were also added and averaged to get mean values at the boundary in row forming 55 rows. At the end of this manual merging method a total of 109 magnetic values in column and 55 values of rows were got giving a total of 55 by 109 magnetic values (5995). These values were keyed into the computer as the unified dataset for this research work.

3.2   Production of the Unified Aeromagnetic Map of the Study Area

The unified dataset are magnetic values without coordinates. Thus before a unified map was produced from these data sets, a computer programme was applied which read the data points row by row and calculated their latitude and longitudes using base values already supplied in aeromagnetic way. The output is in form of column of x, y, z, where x, y, and z represent longitude, latitude and the magnetic value of the given data point respectively, the output file in column x, y, z were then used as an input file for a computer contouring package (SURFER) which produce a unified aeromagnetic map of the area as shown in Figure 3.2
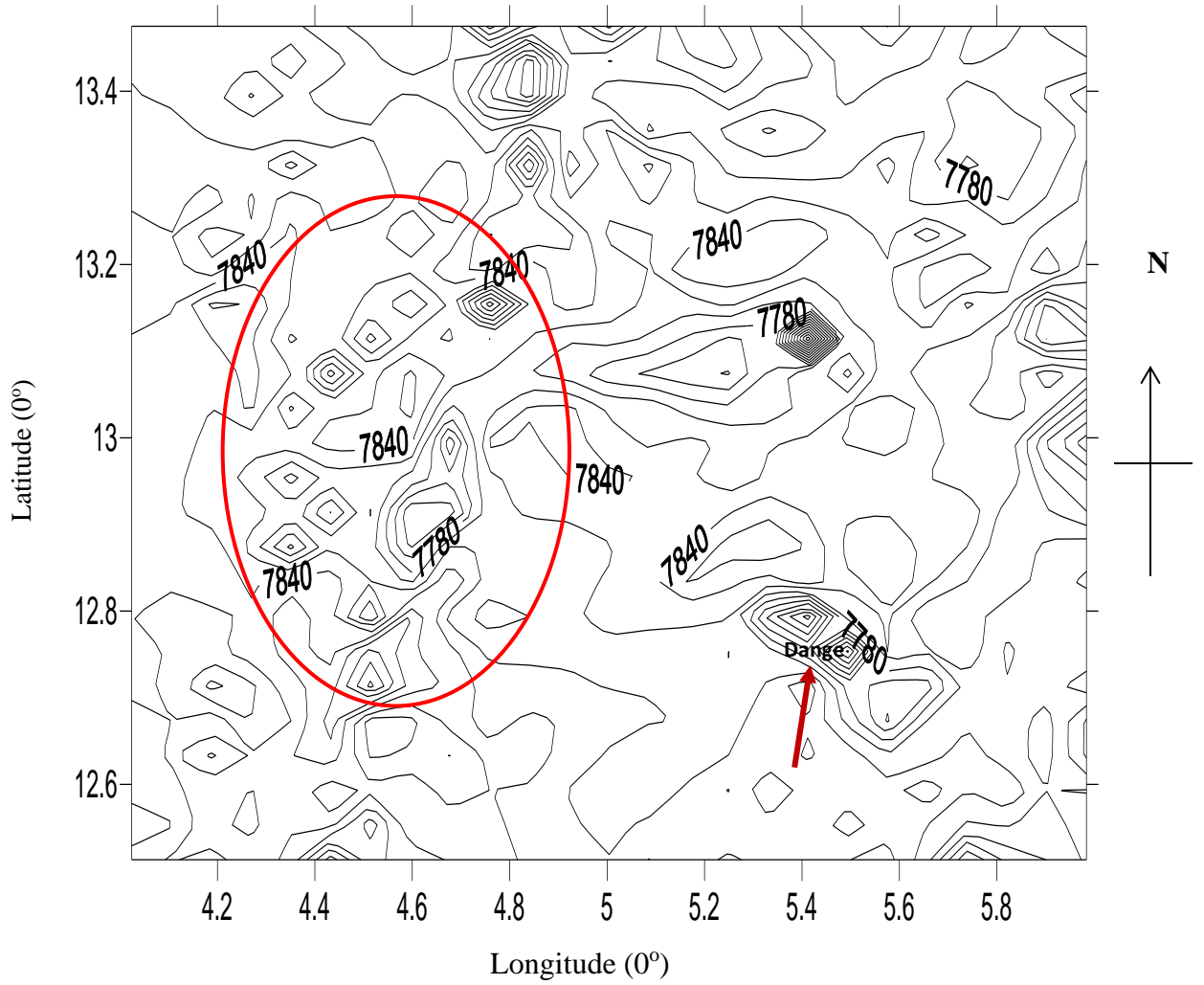
Figure 3.2   **Total Composite Aeromagnetic Map of the Upper Sokoto Basin**

3.2.1   Description of the Magnetic Anomalies in the Study Area

Reviewing of the contoured aeromagnetic map of the Sokoto Basin in Figure.3.2 shows that the magnetic field over the study area has distinct trend.

Closures of the magnetic lows scattered over the western part of Sokoto and prominent among the magnetic lows is NW-SE trending. Closures of sudden gradients and short wavelength occur at western part of Sokoto.

A critical look at figure 3.2 shows that a high frequency magnetic anomaly that is circularly shaped is situated in the North-western part of Dange. South-western of Dange is characterised by low frequency anomalies with regular shape; this may be attributed to deep-lying basement.

3.3   Regional – Residual Separation

Regional anomalies on the magnetic map frequently are masked by deep - seated structures. These large features generally show up as trends, which continue smoothly over considerable distance. The regional effects correspond to low frequencies, while the residuals correspond to high frequencies.

Superimposed on the regional fields, but frequently camouflaged by them, is the smaller, local disturbances, which are secondary in size but primary in importance. These are the residual anomalies. Usually in magnetics and gravity surveying interpretations, it is the local anomalies that are prime interest and the first step in interpretation is the removal of the regional field to isolate the residual anomalies. The separation procedure which is comparable

to filtering of residual or "noise" from smooth regional effect is achieved by either of the two methods of graphical or analytical. There are several ways of removing the regional:

(a)   Graphical and Smoothen method

(b)   Analytical Method

(c)   Polynomial fitting Method

(d)   The Least Square Method

3.3.1   Graphical and Smoothing Method

Visual smoothing method is the earliest method for estimating the regional effect by means of smooth curves on profiles or smooth contours on maps. The method works incompletely by following approximations in the following way. The first step is on look for the local uninterrupted areas where they intersect the irregular contours. The regional trend shown by the extrapolated line is then subtracted from the observed trend at the point of intersection. The result produces the residual field; the flexibility of this method is an advantage because it permits the interpreter to include his own finding about the form of the residual anomalies.

This method will be okay when the regional trend is fairly marked from the beginning. The use of this method which personal bias is subjective, requires considerable work and can be expensive but it is entirely reasonable (Grant and West,1965) the natural subjectivity may either be an advantage or a disadvantage depending on the interpreter's experience and ability to include appropriate geological information about the regional field.

Situations under which the smoothing method cannot be used including:

1. When the ground is hilly and the subsurface materials are in homogenous.

2. When the regional trend is very strong, residual anomalies are easily missed by visual methods.

3. When the ground is not hilly but residual anomalies are very large the regional trends are often very difficult to separate. This is usually true in large scale surveys.

3.3.2 Analytical Methods

These are mathematical procedures, which have been established as improvement over the simple experimental grid system. In this method of finding residual anomalies, numerical procedures on the observed data make it possible to separate anomalies without such a great confidence upon the exercise of judgment in carrying out the separations, it requires that magnetic values be spaced in a regular selection. Some of the rarely used analytical methods are:

1. Direct calculation of residuals by techniques such as the centre-point and ring method.

2. Determination of second derivatives

3. Downward continuation

The direct calculation of residual by centre-point and method involves the calculation of the residual directly from a regular grid of field observations. It involves the averaging of field values along the periphery of a circle or regular polyhedron with its centre at the point for which the residual is to be computed (Dobrin, 1976). The average value around the circle is simply the arithmetic means of a finite number of equally spaced points about its circumference. The residual value is in the choice of a radius and the spacing of sampling

points around the circumference is also arbitrary. Owing to the complex nature of the contours involved, both of these problems are hardly useful in magnetic studies.

Second vertical derivative of magnetic field map is a measure of the curvature of the field, i.e. it enhances geologic features which generate greater curvature of magnetic field. This is the case of anomalies from geological features that are close to the surface. Thus, it enhances weaker local anomalies. Secondly, this method can often be used to delineate the contacts of lithology's with contrasting physical properties such as densities, susceptibilities, etc. (Bhattacharyya, 1966; Henderson and Zietz, 1967). From the aforementioned, this method will not be suitable. Similarly, upward and downward continuation technique cannot be used since we are dealing with total intensity field (F) which is not vertical (Dobrin, 1976). Hence, the polynomial fitting method will be applied in the present study.

3.3.3   The Polynomial Fitting Method

The polynomial fitting method for determining regional magnetic fields presupposes that the residual field has a normal (Gaussian) distribution. However, in the field data many points do not fit this presumed Gaussian model. These data points, which do not fit the normal distribution, model for least-squares estimation, because a distortion of the regional field fitted to the data by the least-squares method (Kangkolo, 1996). This method of matching of regional by a polynomial surface of low order exposes the residual feature as random errors. The surface with closest fit to the magnetic field which is of low order effect, could be well approximated by a low order polynomial are regional fields obtained within a specified degree of detail while the residual is the difference between the magnetic field value as actually mapped and the regional field value thus determined.

3.3.4　The Least Squares Method

Least square operation is an operation which determines the potential surface that fits a given observed magnetic map. The closeness of the fit depends on the degree or order of the calculation.

The least square method has the following advantages over others direct methods of interpretation:

1. Many points of the maps or profiles are used to obtain the solution.
2. Bodies of arbitrary shapes are considered.
3. The solution may take known geological structure into consideration.

Solution can be made simultaneously for anomalies caused by more than one body.

The polynomial coefficients were used to compute the regional map of the study area, the resultant map in Figure 3.3 the regional map trends NW-SW. An acquired program (FORTAIN) was used to derive the residual magnetic values by subtracting values of the regional from the total magnetic values at grid cross points. The contour map of the residual values is shown in   Figure 3.4. These residual anomalies contain the components of the field which presumably are caused by the geological disturbances of interest.
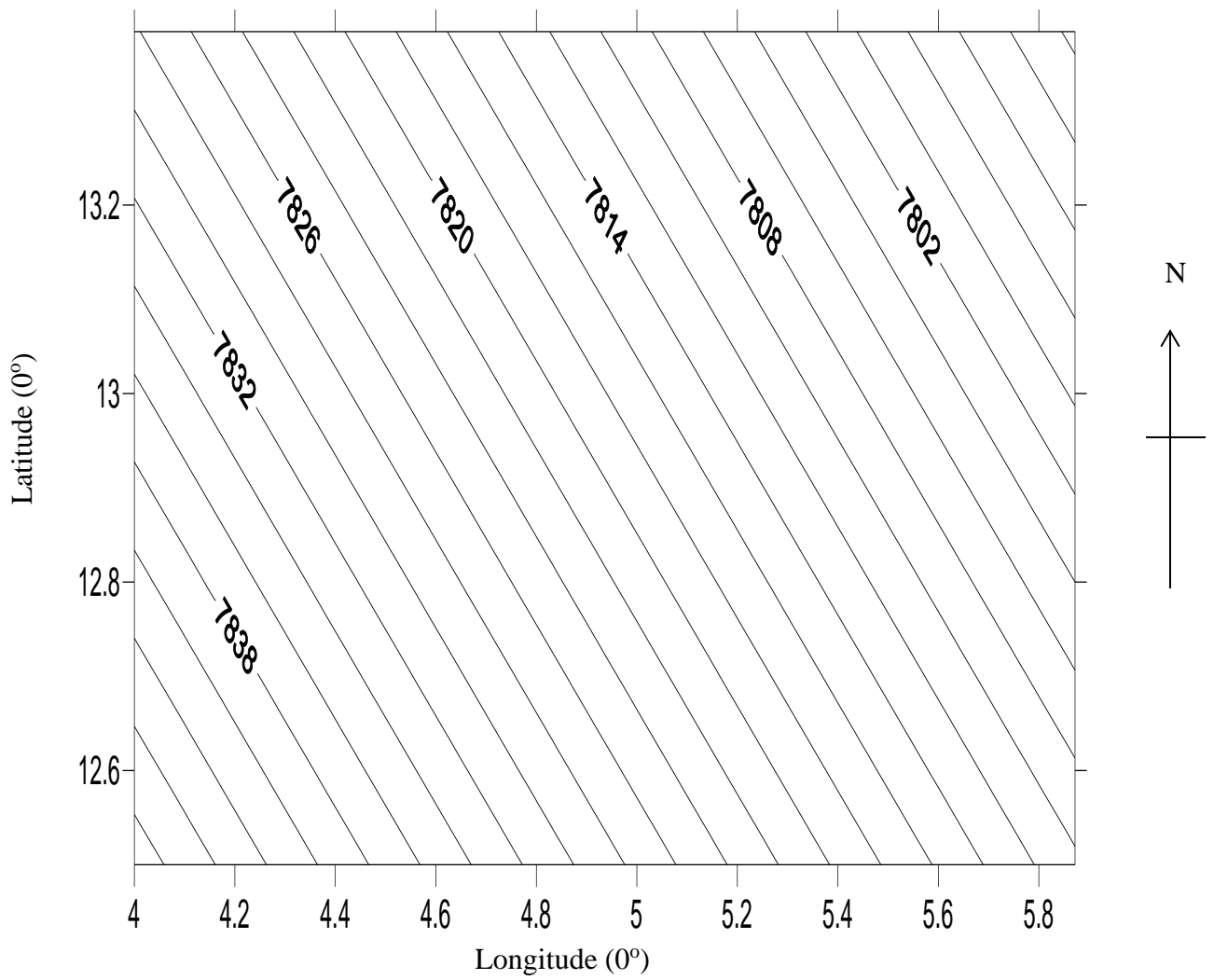
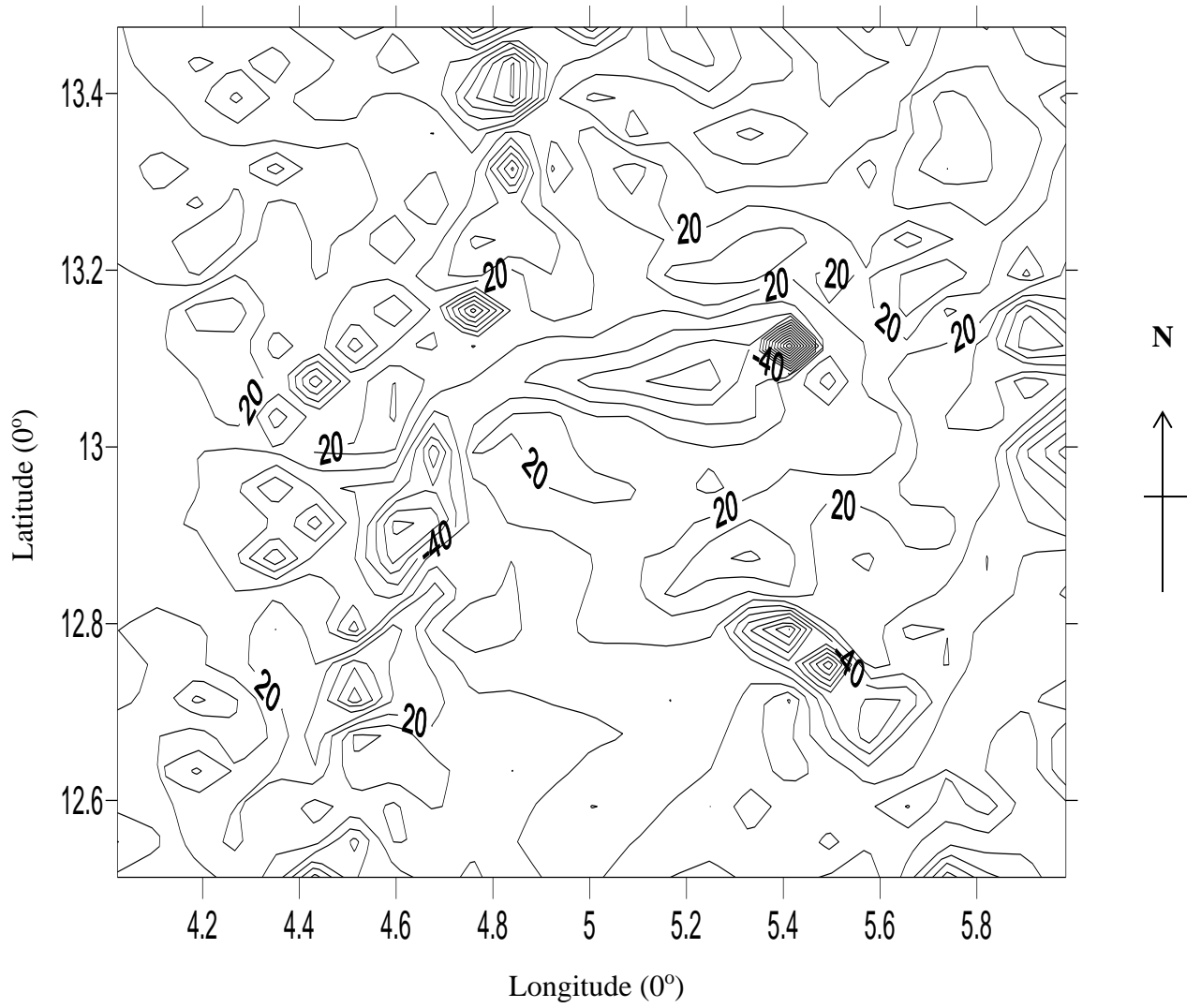**Figure 3.3   The Regional Magnetic Map of the Study Area**

Figure 3.4   The Residual Magnetic Map of the Study Area

3.4   Spectral Determination Method

Spectral analysis of the residual field data can be used to decide thickness of magnetic rocks. The depths are generally computed from field observations made on the width and slopes of separate anomalies. Residual total magnetic field intensity values are used to attain the two-dimensional Fourier series consisting of various frequencies which describe the anomalies. It has been acknowledged recently that a statistically oriented method is desirable because more than one anomaly can be used to estimate thickness of magnetic rock and mean depth values to major units of buried magnetic rocks. This method has been found to yield good estimates of mean depth to the basement underlying a sedimentary basin (Treital *et al.,* 1971; Hahn *et al.*, 1976).

Generally, arithmetical spectral analysis of geophysical phenomena in the right sense of it barely began before large capacity electronic computers came into more general use. And this was within the last years, Spector and Grant, (1970) established depth determination methods by assuming a number of groups of rectangular sided parallelepipeds calculated two dimensional power spectra from the gridded total intensity magnetic field data and matched them with corresponding spectra from a theoretical model (Hahn *et al*., 1976).

This was completed by Fourier transforming the digitised aeromagnetic data over a square, and the computed amplitude spectrum was plotted on a logarithmic scale against frequency. In the present study, a similar method called statistical spectra method was used, Residual total magnetic field intensity values are used to obtain the two dimensional Fourier Transform (Oppenheim and Schafer 1975; Cooley and Turkey 1965).

3.4.1 Fundamentals of Spectral Analysis

The magnetic field value is a function of two space variables X and Y, due to vertical field and horizontal field. The dimensions of the area along both X and Y is normally finite and two consecutive points of the digitised data spaced apart by finite interval. It is likely to present this data perfectly by a two dimensional Fourier series which is limited by lower and upper frequency limits because of the finite dimensions of the selected area on one hand and the finite station spacing on the other.

The Fourier series comprises of terms of diverse frequencies that combine together to form the potential field data. The amplitude and phase relationships among these frequencies constitute what is called ''Complex Line Spectrum'' (Negi *et al.,* 1983). These relationships govern the way the Fourier series is built up (Bhattacharyya, 1966) and it has been used extensively by various workers for the interpretation of gravity and magnetic data.

A periodic function f(x) of the independent variable X, the dimension of which is length, may be expressed as a Fourier series as below

$$f(x) \frac{a_o}{2} + \sum_{n=1}^{\infty} \left(a_n \cos n\omega x + b_n \sin \omega x \right) \qquad 3.1$$

Where ω is the fundamental angular frequency given by $\omega = 2\pi/x$ where x is the total length of x over which f(x) has been measured. The coefficients a_n and b_n are given below.

$$a_n = \frac{2}{x} \int_{\frac{x}{2}}^{x/2} f(x) \cos n\omega \, xdx$$

And $b_n = \dfrac{2}{x} \int_{\frac{x}{2}}^{x/2} f(x) \sin n\omega\, xdx$

Expressed in the exponential form Equation 3.1 may be written as

$$f(x) = \sum_{n=1}^{\infty} f(x)n)e^{jn\omega x}\, dx \qquad\qquad 3.2$$

And

$$F_{(n)} = \dfrac{1}{x} \int_{\frac{x}{2}}^{x/2} f(x)\ e^{jn\omega x}\, dx \qquad\qquad 3.3$$

When the period x is allowed to tend to infinity, the function f(x) begins to approach on a periodic function or a transient function which contains all possible frequency. In such a case the summation in the series equation 3.2 is replaced by an integral and equation 3.2 reduces to

$$F(x) = \dfrac{1}{2\pi} \int_{\infty}^{\infty} (x)\, l^{jn\omega x}\, d\omega \int_{\infty}^{\infty} f(\sigma) l^{-j\omega\sigma\, d\sigma} \qquad\qquad 3.4$$

$$F(\omega) = \int_{\infty}^{\infty} f(x) l^{-j\omega x\, dx}$$

And

$$F(x) = \dfrac{2}{2\pi} \int_{\infty}^{\infty} f(\omega)e^{j\omega x}\, d\omega \qquad\qquad 3.5$$

From the equation (3.5), it is evident that the periodic function f(x) may be thought of as a synthesis of an infinite aggregate of sinusoid e^{jwx} of all angular frequencies ω in the continuous infinite range $(-\infty, \infty)$ having a complex amplitude F (ω). This function F (ω) is the complex continuous spectrum of a periodic function F(x). Equation (3.5) and (3.6) are called Fourier Transforms Applying Fourier Transforms on the two cases. Qs 3.5 and 3.6 becomes

$$G (u \cdot v) = \int_{-\infty}^{\infty} \int_{-\infty}^{\infty} g(x,y) l^{\,j(ux+vy)} dx dy$$

and

$$g(x,y) = \frac{1}{4\pi^2} \int_{-\infty}^{\infty} \int_{-\infty}^{\infty} G(u,v) l^{\,j(uv+vy)} dx dy$$

Where u and v are the angular frequencies in the x and y direction respectively

$$G (u, v) = P (u, v) + JQ (u, v) \qquad\qquad 3.8$$

The amplitude spectrum of G (u , v) is

$$A (u , v) \; = |G(u,V)| = \; |P^2 + Q^2|^{\,1/2} \qquad\qquad 3.9$$

And its phase spectrum is

$$\theta (u,v) = are \tan (Q/P) \qquad\qquad 3.10$$

The energy density spectrum or the energy spectrum is

$$E (u,v) = |G(u,V)|^{\,2} = (P^2 + Q^2) \qquad\qquad 3.11$$

For the treatment of sample data the discrete form of G (u,v) has to be employed. Generally, the discrete Fourier Transform pair for the two dimensional data sequence g (m,n) which is

zero outside the interval $0 \leq m \leq m - 1, 0 \leq n \leq N - 1$ is given by (Oppenheim and Shafer,

1975); $G(KL) = \sum_{M=0}^{M-1} \sum_{N=0}^{N-1} g(m,n) \, \omega_m^{km} W_n^{ln}$

$$g(m,n) = \frac{1}{MN} \sum_{k=0}^{M-1} \sum_{L=0}^{N-1} G(K,L) \, \omega_m^{-km} W_n^{-ln} \qquad\qquad 3.12$$

Where $w_m = l^{-\frac{\sqrt{2\pi}}{m}}$ and $w_{n=} l^{-\frac{\sqrt{2\pi}}{n}}$.

3.4.2 Energy Spectrum and Depth to Magnetic Source

The Fourier transform of a selection of magnetic map digitised in a square grid forms a rectangular matrix with coefficients, which can then be reduced to a set of average amplitude dependent only on the frequency (Hahn *et al.*, 1976). These average amplitudes fully represent the spectrum from which the depth to the magnetic source can be estimated. Consider the energy spectrum of the total magnetic field intensity anomaly over a single rectangular block. The expression for the energy spectrum transcribe in solar coordinates is given as follows (Spector and Grant 1970),

If $r = (u^2 + v^2)$ and $0 = $ arc tan (u/v) then the energy spectrum E (r, 0) is given by

$$E(r,0) = 4\pi^2\, K^2\, e^{-2hr}\, (1 - e^{-tr})\, S^2\, (r,0)\, R^2_T\, (0)\, R^2_k\, (0) \qquad\qquad 3.13$$

Where

K is the magnetic moment per unit dept.

$$S_{r,0} = \frac{\sin (ar\ \text{Cos} (0)}{ar\ \cos(0)}\quad \frac{\sin (br\ \text{Cos} (0)}{br\ \cos(0)}$$

$$R^2_T (0) = \left| n^2 + (1\ cos\ (0) + m\ sin\ (0)\ ^2 \right|$$

$$R^2_k (0) = \left| N^2 + (L\ cos\ (0) + M\ sin\ (0)\ ^2 \right|$$

L, m, and n are direction cosines of the magnetic moment vector.

For the purpose of analysing aeromagnetic maps, the ground is assume to consist of a number of independent ensembles of rectangular, vertical sided parallelepiped, and each ensemble is characterised by a joint frequency distribution for the depth 'h' width 'a' and length 'b'. The overlapping sections consist of super position of large number of individual anomalies

overlapping due to several ensembles of blocks having various dimensions and magnetisations.

The energy spectrum of the double ensemble will consist of two parts. The first which relates the deeper sources is relatively strong at the low frequencies and decays away rapidly. The second which arises from the shallower ensemble of sources, dominates the high frequency end of the spectrum.

Spector and Grant, (1970) obtained the expression for the ensemble average of the radial spectrum as

$$< E\ (r)\ > = 4\pi^2 K^2 < l^{-2hr} >< (1\text{-}l^{tr}\ )^2 >< S^2(r)> \qquad\qquad 3.14$$

$$<S^2(r)> = \frac{1}{\pi} \int_0^\pi < S(r,0) > d0 \qquad\qquad 3.15$$

The ensembles average depth 'h' enters only into the factor

$$< l^{-2hr>} \quad = \frac{l^{-2hr>} \sin h\ (2r\triangle\theta}{4r\triangle h} \qquad\qquad 3.16$$

Depth to magnetic rock estimation for magnetic field data can be approximated to exp (-2hr) (Spector and Grant, 1970). This shows that the radial spectrum may be conveniently approximated by a straight line segment, the slopes of which relate to the depth of the possible layers (Spector and Grant 1970; Naidu, 1970; Hahn *et al*., 1976).

The residual magnetic field intensity values are used to obtain the two dimensional Fourier from which the spectrum is to be extracted.

From the residual values $\triangle T\ (x,Y)$ consisting of M rows and N columns in the x y plane,

the two dimensional Fourier transform obtained in Equation 3.12 above and the evaluation is done using an algorithm that is a two dimensional extension of the Fourier transform (Openheim and Schafer. (1975), Cooley and Turkey, 1965).

Then, the frequency intervals are subdivided into sub-intervals, which lie within one unit of frequency range is calculated and the resulting values together constitute the redial spectrum of the anomalous field (Hahn *et al.,* 1976; Negi 1983; Kangkolo 1996)

The natural logarithms of the radial spectrum for each block were then plotted against frequencies. These plots showed a series of points that may well be represented by straight lines (linear segments). Most of the point due to anomalies caused by the bodies occurring within a particular depth range or at different levels fall on one or more straight line segments whose slopes can be used to determine the mean depths to the assemblage of anomalous bodies (Spector and Grant, 1970 and Hahn, *et al.,* 1976). The first few point of low frequency components in the spectral graph were generated from the deepest layers whose locations most likely in error were ignored, since it has been established that error depth estimation increases with depth of source and is also related to the aeromagnetic map size (Pal *et al.*, 1978). The slope of the segments is related to the depth as follows (Spector and Grant, 1970):

$$D = -m/2 \qquad\qquad 3.15$$

Where D is the mean depth of the burial of ensemble and m is the slope of the line of best fit Equation 3.15 is the basic equation for the slope-depth relation for power spectrum analysis and can be applied directly if the frequency Unit is in radian per kilometre. If however the frequency unit is in cycles per kilometre.

The corresponding relation is expressed as

$$D = -m/4\pi \qquad\qquad 3.16$$

The use of Discrete Fourier Transform introduces the problems of aliasing and the truncation effect (or Gibb's Phenomenon). Aliasing was reduced by the digitising interval used in this study. The truncation effect was reduced by applying a cosine taper to the observed data Fourier transformation (Bath, 1974; Kangkolo, 1996).

Considering equation 3.13 and 3.14 again, the estimation of the thickness contribution to the energy spectrum is given as:

$$[C^2 (t, r)] = [1 - e^{-tr}]^2 = 1 - (3 - e^{-2tr})/4tr \qquad\qquad 3.20$$

The parameter t (i.e. thickness) plays a rather interesting role in shaping the power spectrum when combined with the depth factor e-^{2hr} (for not too large values of r), the effect of $[C^2(t, r)]$ is to produce a peak in the spectrum whose position shifts towards smaller wavenumbers with increasing value of t when this peak occurs (significant maximum), indicating that the source bottom are detectable, the wavenumber f_{max} of the spectral peak , the mean depth D to the sources tops and the mean depth D to the source bottom (base depth) are related by (Boler, 1978; Connard *et al.*, 1983; Salem *et al.*, 2000):

$$f_{max} = \frac{1}{2\pi(d-Z)} \text{ in d/z} \qquad\qquad 3.21$$

Where d = Z + t

Whether the source appears to be depth limited or not depends very much on the size of the map. The longest wavelength for which the Fourier Transform can be calculated is the total

depth information down to a depth of length L/2π (Shuey *et al.,* 1977), if the source body have bottom deeper than L/2π, the spectral peak occurs at a wavenumber lower than the fundamental wavenumber for the map and cannot be resolved by the spectral analysis. When a significant maximum occurs, indicating that the source bottoms are detectable, equation 3.21 applies.

3.4.3   Curie-Point Depth Estimation from Magnetic Centroid

Estimate of the thickness of the magnetised portion of the earth's crust suggest that there are two types of lower boundaries of the layer of magnetised rocks. The first type of boundary corresponds to vertical changes in crustal composition. In areas characterised by normal and low heat flow, the bottom of the bodies causing regional magnetic anomalies seems to coincide with intracrustal seismic discontinuities suggesting a lithological interface (Connard *et al.,* 1983). The second type occurs where high temperature at various depths causes the rock to lose their ferromagnetic properties that is below Curie point depth (Connard *et al.*, 1983).

Thus the Curie-point depth is the depth at which dominant magnetic minerals reach a temperature of $580^{o}C$ or $300^{0}C$, which is the temperature such rocks lose their magnetic properties. The Curie point depth is estimated in two steps as suggested by (Bhattacharyya and Leu, 1975; Okubo *et al.*, 1985).The first is the depth to the Basement (D_2) of the magnetic source, from the slope of the longest wavelength part of the spectrum,

$$\text{In} \left[\frac{P(s)^{1/2}}{|S|}\right] = \text{ln A} - 2\pi|s| \, D_2 \qquad\qquad 3.22$$

Where P(s) is the radially averaged power spectrum of the anomaly, |s| is the wavenumber, and A is a constant .The second step is the estimation of the depth to the Centroid (D_3) of that

distribution from the slope of the second longest wavelength spectral segment (Okubo *et al.,* 1985)

$$\ln[P(s)^{1/2}] = \ln B - 2\pi |s| D_3$$

Where B is a sum of constants independent of |s|, then the basal depth (D_b) of the magnetic source is calculated from the equation

$$D_b = 2D_3 - D_2 \qquad\qquad\qquad 3.23$$

Bottom depth D_b can only be estimated if centroid (D_3) can be accurately determined.

The study area was divided into twenty-four (24) cells for the purpose of spectral and geothermal analysis. Graph of the logarithm of the spectral energies against their corresponding wavenumbers for each cell are shown in appendix, and equation 3.23 was used to estimate the depth to the causative body (curie-point isotherm) i.e. deep and shallow sources. From the earth's surface downward, the depths are shown on Table 3.2 Consequently; contour maps of the deeper and shallow depth with their corresponding 3-D surface models were produced and are shown in Figure 3.5 - 3.8. The ground surface is regarded as being at a depth of zero kilometres.

Table 3.2: Estimated Depth to the Centroid (D_3), Basement (D_2) Magnetic Sources

| S/NOS	SECTIONS	LONGITUDE (^{o})	LATITUDE (^{o})	DEPTH (LAYER 3) D_3(km)	DEPTH (LAYER 2) D_2(km)
1	SEC 1	4.125	13.375	5.495	0.58
2	SEC 2	4.375	13.375	4.995	0.53
3	SEC 3	4.625	13.375	4.485	0.78
4	SEC 4	4.875	13.375	4.655	1.26
5	SEC 5	5.125	13.375	6.265	1.625
6	SEC 6	5.375	13.375	3.760	1.74
7	SEC 7	5.625	13.375	7.255	1.58
8	SEC 8	5.875	13.375	3.855	1.665
9	SEC 9	4.125	13.125	3.840	1.325
10	SEC 10	4.375	13.125	4.455	1.77
11	SEC 11	4.625	13.125	8.110	1.38
12	SEC 12	4.875	13.125	8.020	1.21
13	SEC 13	5.125	13.125	3.080	1.375
14	SEC 14	5.375	13.125	3.935	1.785
15	SEC 15	5.625	13.125	3.720	1.345
16	SEC 16	5.875	13.125	3.495	1.27
17	SEC 17	4.125	12.375	4.060	1.09
18	SEC 18	4.375	12.375	4.160	1.135
19	SEC 19	4.625	12.375	3.650	1.335
20	SEC 20	4.875	12.375	4.440	1.19
21	SEC 21	5.125	12.375	3.830	1.045
22	SEC 22	5.375	12.375	4.025	1.07
23	SEC 23	5.625	12.375	5.680	0.505
24	SEC 24	5.875	12.375	4.315	1.175
	AVERAGE VALUES			**4.763**	**1.240**
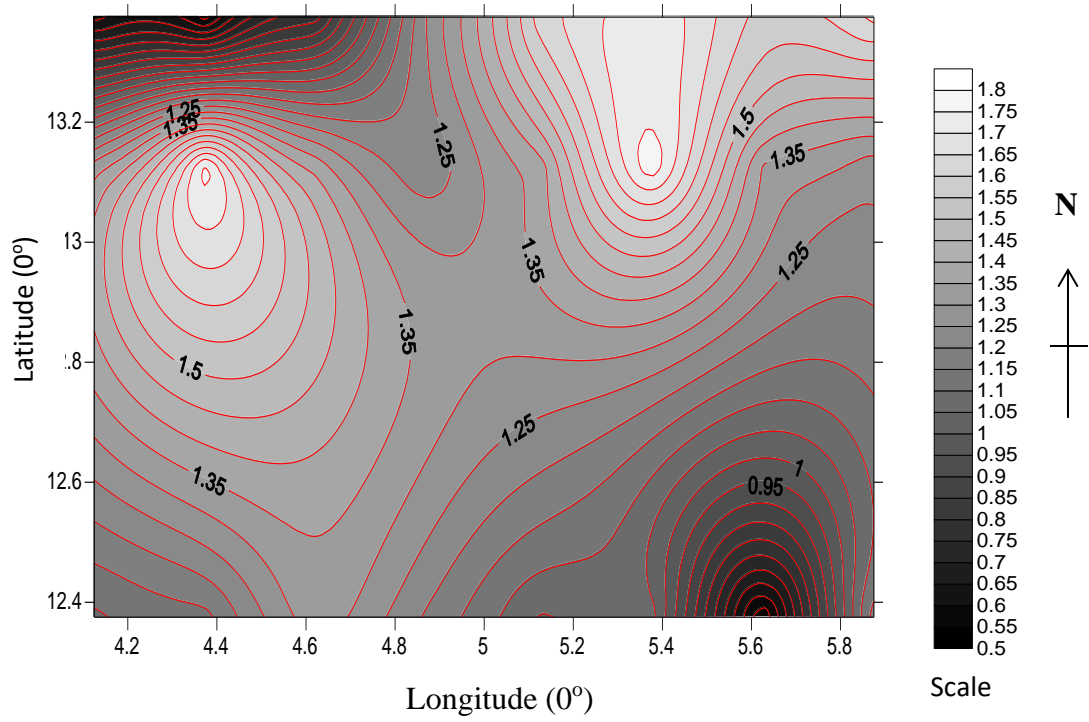
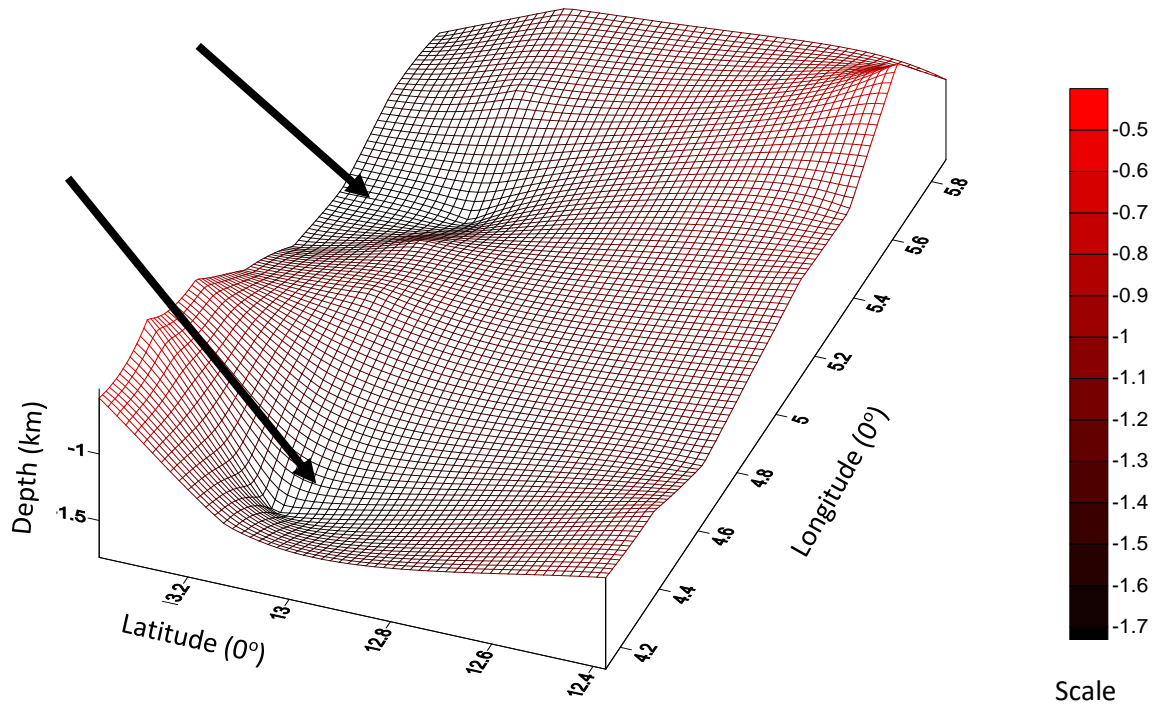**Figure 3.5   Contour Map of Depth to Basement D₂ in km.**

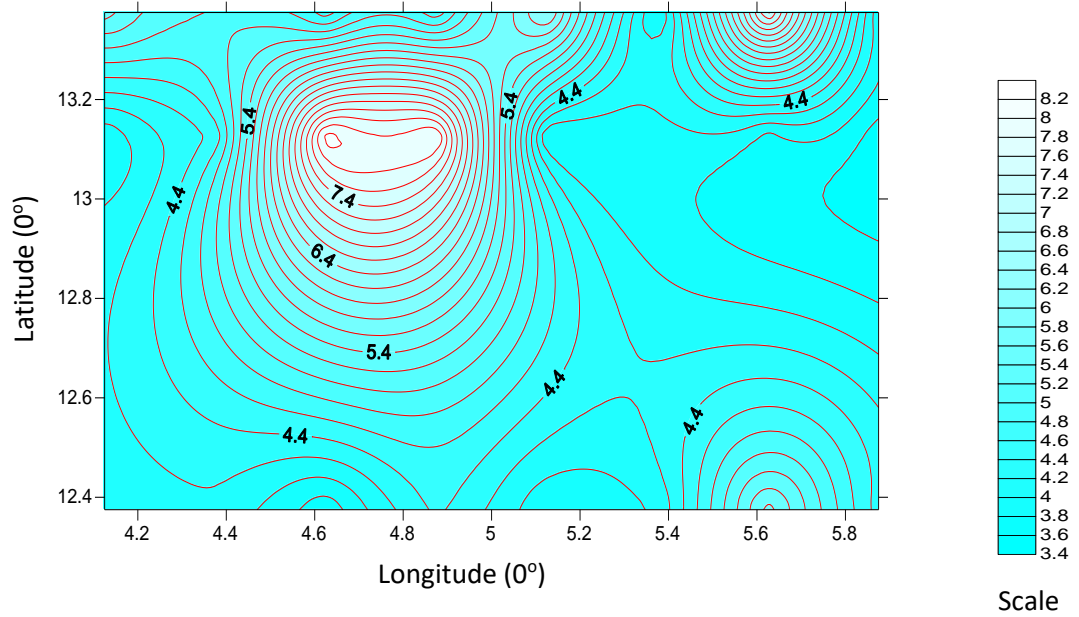**Figure 3.6. 3-D Model Surface Plot of Depth to Basement D₂ in km.**

Figure 3.7 Contour Map of the Centroid depth D_3 in km.
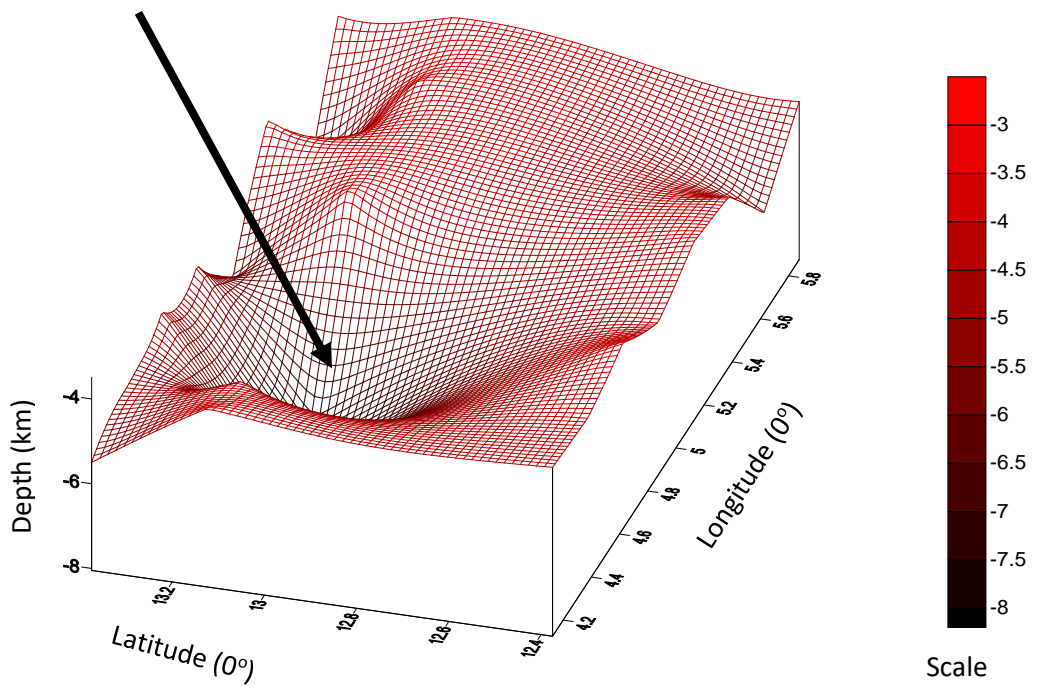

Figure 3.8   3-D Model Surface Plots of Centroid depth D_3 in km

The magnetic field observation made at or above the surface of the earth and the magnetisation at the top of the magnetic part of the curst are characterised by relatively short spatial wavelength, while the magnetic field from the magnetisation at the curie-point depth will be characterised by longer wavelength and lower amplitude magnetic anomalies (Bhattacharyya and Leu (1975).

The obtained basal depth of a magnetic source is assumed to be Curie point depth.

The Table below also gives the curie-point depth estimated from the analysis of the frequency of the spectral maximum. Subsequently, contour map of the curie- point depth and its corresponding 3-D Model were generated and showed in Figure 3.9 and 3.10 respectively. The estimated depth to curie-point in this area varies from 5.72 km to 14.84 km with average of 8.2848 km. Previous workers such as Connard *et al*., (1983); Bhattacharyya and Leu (1975) have indicated that the curie – point depth is mostly dependent on the geological setting of the area under consideration.

Table 3.3: Estimated Depth to the Curie point D_b

| S/NOS	SECTIONS	LONGITUDE (^{0})	LATITUDE (^{0})	DEPTH (LAYER 3) D_3(km)	DEPTH (LAYER 2) D_2(km)	CURIE POINT D_b (km)
1	SEC 1	4.125	13.375	5.495	0.58	10.41
2	SEC 2	4.375	13.375	4.995	0.53	9.46
3	SEC 3	4.625	13.375	4.485	0.78	8.19
4	SEC 4	4.875	13.375	4.655	1.26	8.05
5	SEC 5	5.125	13.375	6.265	1.625	10.905
6	SEC 6	5.375	13.375	3.760	1.74	5.78
7	SEC 7	5.625	13.375	7.255	1.58	12.93
8	SEC 8	5.875	13.375	3.855	1.665	6.045
9	SEC 9	4.125	13.125	3.840	1.325	6.355
10	SEC 10	4.375	13.125	4.455	1.77	7.14
11	SEC 11	4.625	13.125	8.110	1.38	14.84
12	SEC 12	4.875	13.125	8.020	1.21	14.83
13	SEC 13	5.125	13.125	3.080	1.375	6.225
14	SEC 14	5.375	13.125	3.935	1.785	6.085
15	SEC 15	5.625	13.125	3.720	1.345	6.095
16	SEC 16	5.875	13.125	3.495	1.27	5.72
17	SEC 17	4.125	12.375	4.060	1.09	7.03
18	SEC 18	4.375	12.375	4.160	1.135	7.185
19	SEC 19	4.625	12.375	3.650	1.335	5.965
20	SEC 20	4.875	12.375	4.440	1.19	7.69
21	SEC 21	5.125	12.375	3.830	1.045	6.615
22	SEC 22	5.375	12.375	4.025	1.07	6.98
23	SEC 23	5.625	12.375	5.680	0.505	10.855
24	SEC 24	5.875	12.375	4.315	1.175	7.455
	AVERAGE VALUES			**4.763**	**1.240**	**8.285**
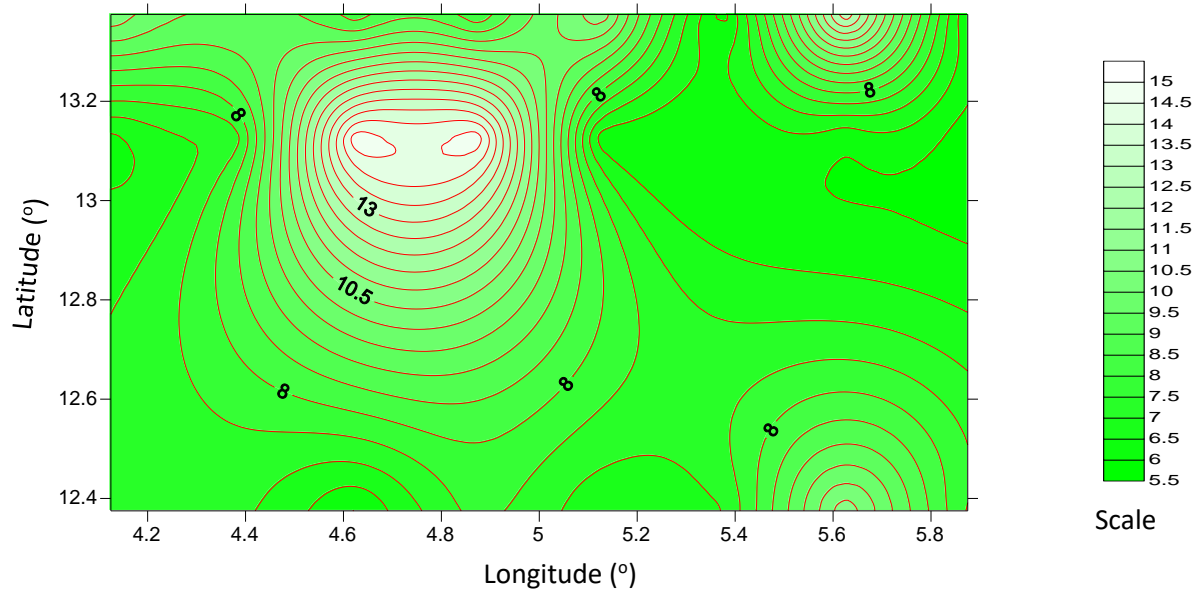
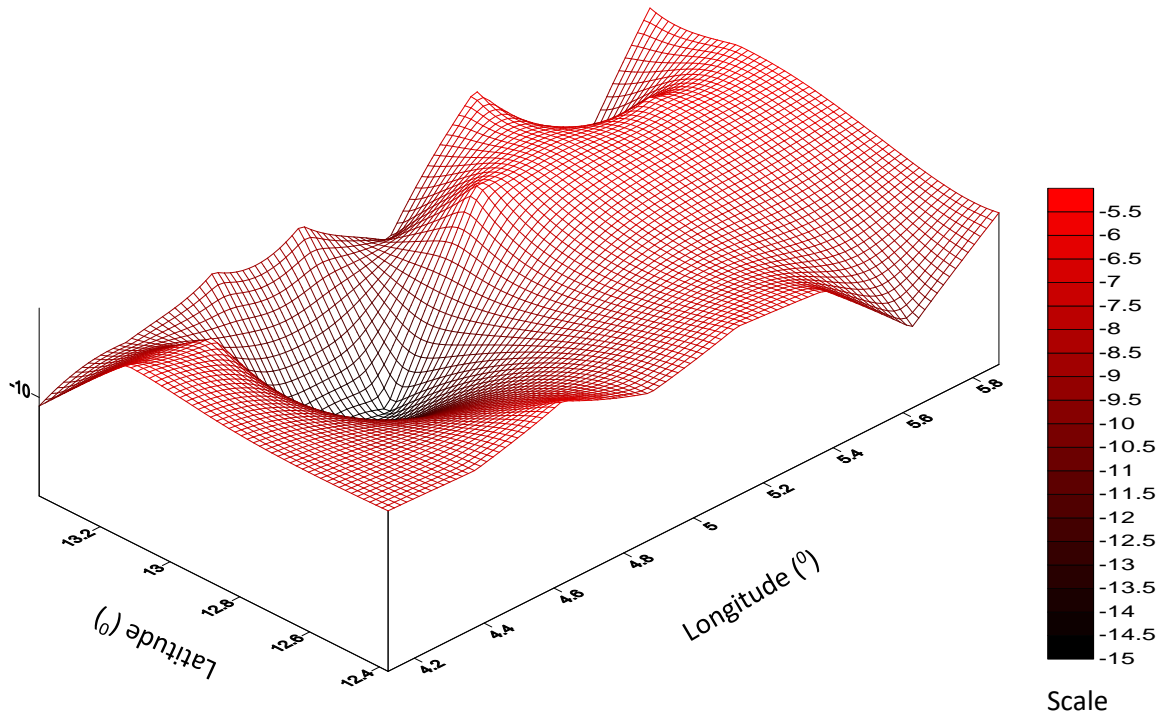Figure 3.9: **Contour Map of the Curie point depth in km**

Figure 3.10 **3-D Model Surface Map of the Curie poi**

3.5   Geothermal Gradient

Geothermal gradient is the change in temperature increase with depth into the earth's surface. The heat flow ……………….q, which directs this variation, is express by Fourier's law given by;

$$q = \lambda \frac{dT}{dD}$$ 3.24

Where, λ is the coefficient of thermal conductivity. In this equation, it is assumed that the direction of the temperature variation is vertical and the temperature gradient $\frac{dT}{dD}$ is constant. The average temperature increase is 25°C per kilometre of the depth. However some regions have much higher gradient indicating concentration of heat at shallow depths. Such regions could have potentials for generating geothermal energy (Plummer *et al.,* 1999).

According to Tanaka *et al*., (1999), the Curie temperature (Θ) can be obtained from the Curie-point depth (D_b) and the thermal gradient dT/dD using the following equation;

$$\Theta = \frac{dT}{dD} D_b$$ 3.25

In this equation, it is assumed that the surface temperature is 0 °C and no heat sources exist between the Earth's surface and the Curie point depth. In addition, from Equation (3) and Equation (4) a relationship can be determined between the Curie-point depth (D_b) and the heat flow (*q*) as follows.

$$q = \lambda \frac{\Theta}{D_b}.$$ 3.26

In this equation the Curie-point depth is inversely proportional to the heat flow (Turcotte & Schubert, 1982; Tanaka *et al*., 1999; Stampolidis *et al*., 2005).

An average Curie–point temperature of 300°C for crustal rocks is used in this study (Stacey, 1977). However Haggerty (1978) pointed out that Curie-point temperature as low as 300°C may exist in crust because of the low temperature oxidation of titanomagnetic.

3.6   Surface Heat Flow

To determine temperature variation, the primary observable quantity put into consideration is the heat flow. A small but measurable amount of heat from the earth's interior is being lost gradually through the earth's surface. This gradual loss of heat through the earth's surface is called Heat Flow. This heat could be the 'original' heat from the time the earth was formed, that is, if the earth was formed as a hot mass that is now cooling down (Plummer *et al.,* 1999). It could also be a by-product of the decay of radioactive isotopes inside the earth. Some regions on the earth have high heat flow. More heat is being lost through the earth's surface in these regions than is normal. High heat flow is usually caused by the presence of a magnetic body or still cooling down plutons near the surface (Plummer *et al.*, 1999). An old body of igneous rock that is rich in uranium and other radioactive isotopes can cause a high heat flow too, because radioactive decay produces heat as it disintegrate. Warm mantle materials existing beneath abnormally thin crust may also contribute to the high heat flow of an area. In this work, a Curie-point temperature of 300°C and thermal conductivity of 2.0 ± 0.4Wm$^{-1\circ}$C^{-1} as an average for clay stone (Reiter and Jessop, 1985) has been used as a standard (Stacey, 1977).

The corresponding geothermal gradient and surface heat flow values are based on possible Curie-point temperature of 300°C using a conductivity of 2.0 Wm$^{-1\circ}$C^{-1}. Table 3.4 shows the geothermal gradient and heat flow value respectively for the study area. The contour maps and 3-D surface maps for the geothermal gradient and heat flow are equally shown in (Figure 3.11 and 3.14) respectively.

Table 3.4: Estimated values of Geothermal Gradient and Heat Flow

| S/NOS	SECTIONS	LONGITUDE (^{0})	LATITUDE (^{0})	VERTICAL GEOTHERMAL GRADIENT ^{o}C/km	HEAT FLOW qmW/m^2
1	SEC 1	4.125	13.375	28.818	51.873
2	SEC 2	4.375	13.375	31.712	57.082
3	SEC 3	4.625	13.375	36.630	65.934
4	SEC 4	4.875	13.375	37.267	67.080
5	SEC 5	5.125	13.375	27.510	49.518
6	SEC 6	5.375	13.375	51.903	93.425
7	SEC 7	5.625	13.375	23.201	41.763
8	SEC 8	5.875	13.375	49.627	89.330
9	SEC 9	4.125	13.125	47.206	84.972
10	SEC 10	4.375	13.125	42.016	75.630
11	SEC 11	4.625	13.125	20.215	36.388
12	SEC 12	4.875	13.125	20.229	36.412
13	SEC 13	5.125	13.125	48.192	86.746
14	SEC 14	5.375	13.125	49.301	88.742
15	SEC 15	5.625	13.125	49.220	88.597
16	SEC 16	5.875	13.125	52.447	94.405
17	SEC 17	4.125	12.375	42.674	76.813
18	SEC 18	4.375	12.375	41.753	75.156
19	SEC 19	4.625	12.375	50.293	90.528
20	SEC 20	4.875	12.375	39.011	70.221
21	SEC 21	5.125	12.375	45.351	81.632
22	SEC 22	5.375	12.375	42.979	77.363
23	SEC 23	5.625	12.375	27.637	49.746
24	SEC 24	5.875	12.375	40.241	72.434
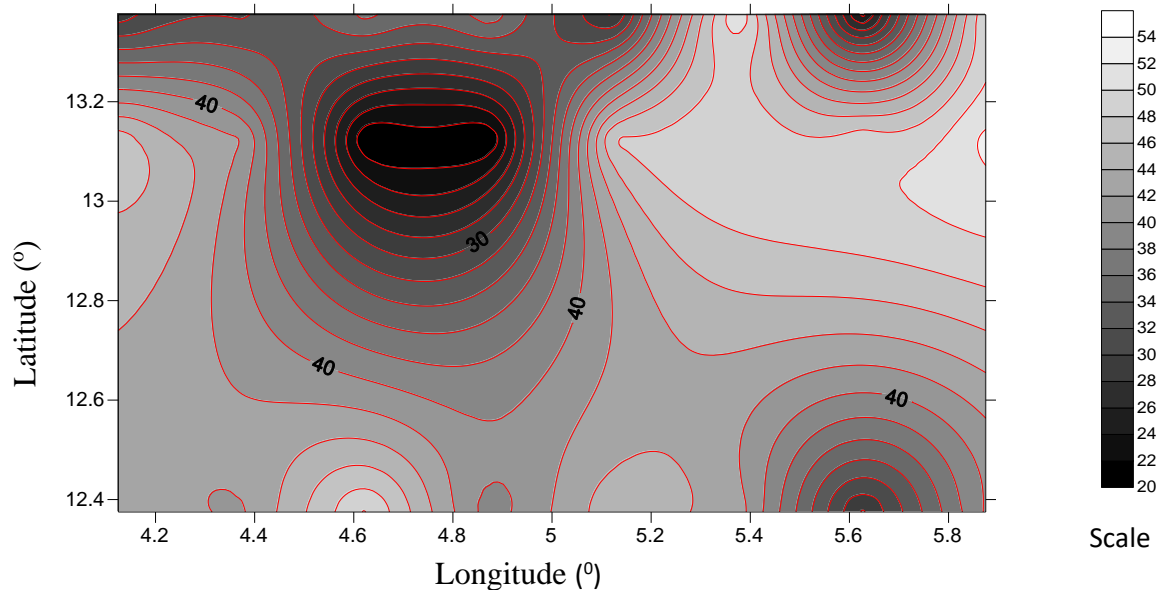
Figure 3.11: Contour Map of Vertical Geothermal Gradient in (^{O}c/km)

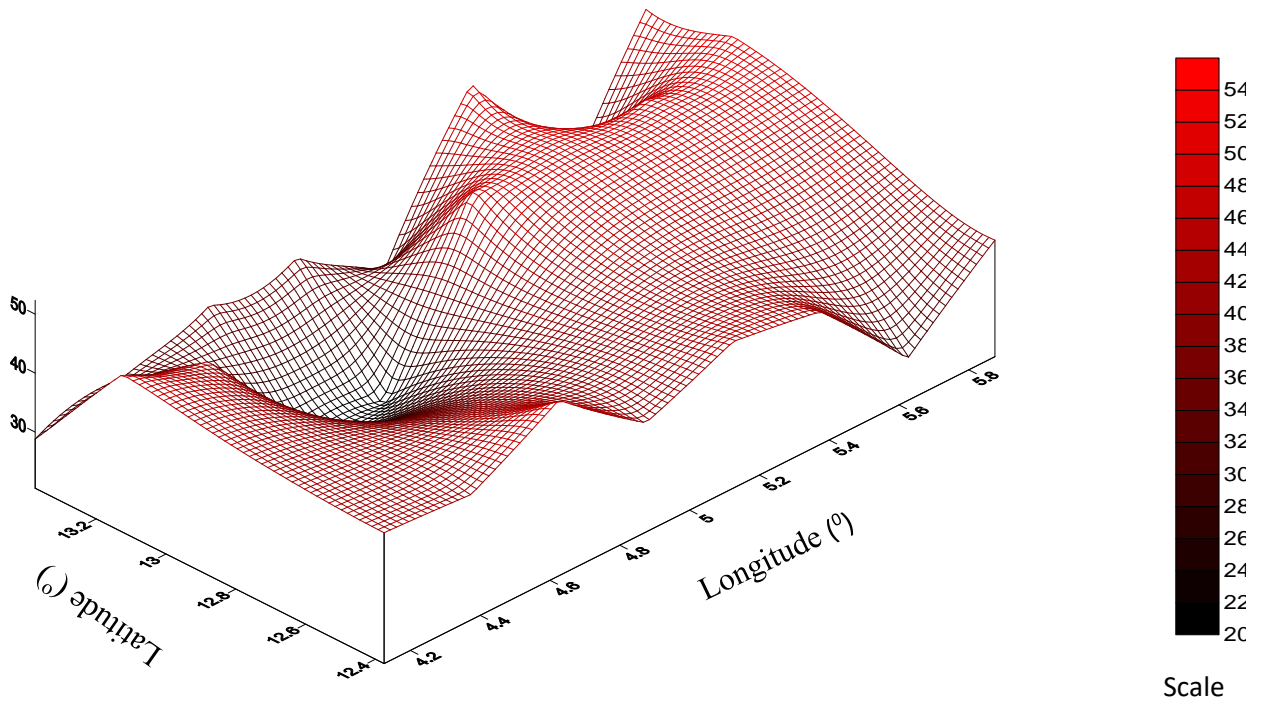**Figure 3.12: 3D Surface Map of Vertical Geothermal Gradient in (^{o}C/km)**

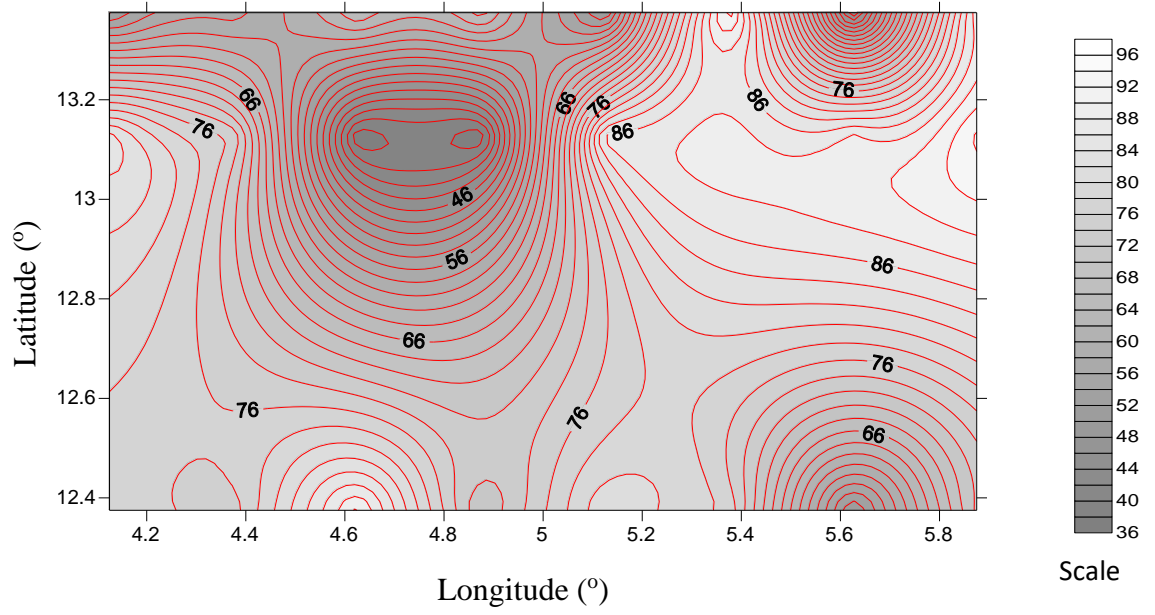**Figure 3 .13   Heat Flow Contour Map**
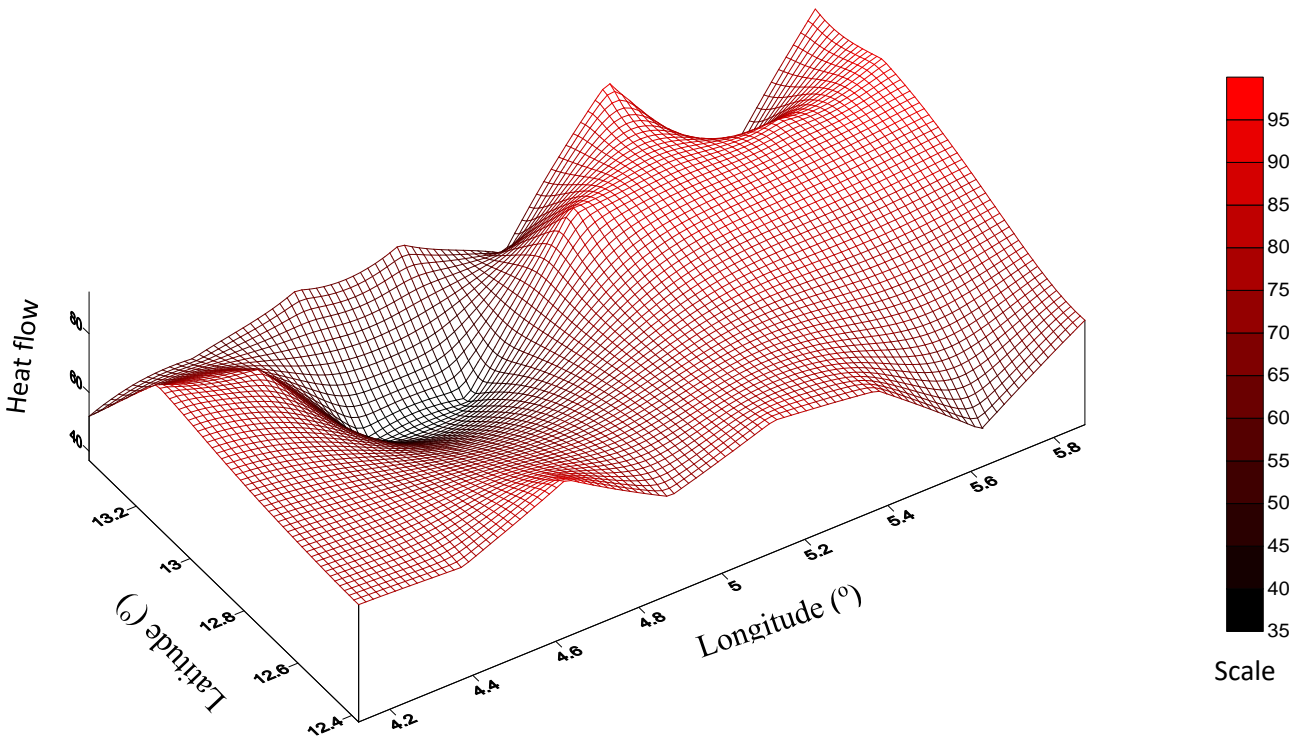

Figure 3.14:   3D Model Surface Map of Heat Flow

CHAPTER 4

4.0   Results and Discussion

4.1   Regional and Residual Map Analysis

The regional magnetic map Figure 3.3 of the study area trends NW-SE while the residual magnetic map Figure 3.4 shows that the magnetic field over the study area shows a NE direction trend which could be seen at the central part of the map and the SE region of the map and generally in other part of the map. Many of the anomalies in the residual magnetic map Figure 3.5 have short wavelengths, small widths and are more or less circular in shape. This is suggestive of shallow intrusive either within the sediments or on the underlying basement surface. Series of closures are easily observed in the residual map with one of the steepest slope existing around the NE portion of the map.

4.2   Spectral Depth Analysis

The total area of the research work is covered between Longitude 4.00°E and 6.00°E and Latitude 12.50°N and 13.50°N, for the determination of spectral depth, the study area was divided up into 24 sections. The locations of these sections are indicated below in tables each section covers a square area of about 28 km x28 km which represents a square grid of 14 x 14 residual field point.

A computer program, SPT 98, was used to estimate the radial range for each subdivision,

Graphs of logarithms of the spectral energies against frequencies obtained for the various sections are shown in appendix. Each of these graphs represents two linear segments. The first point which represents contributions from much deeper sources was disregarded because of the reduced dimensions of these areas covered by these sections. As mentioned earlier, the

gradients of the linear segments were estimated and Equation 3.15 was used to calculate the average depths to the causative bodies from the earth surface downwards. There average depths are shown as D_2 and D_3 in Table 3.3. The Second layer (D_2) varies from 0.505 km to 1.77 km with an average of 1.240 km; this is depth to basement or thickness of sediment. The Third layer (D_3) varies from 3.495 km to 8.110 km with an average 4.763 km, this is the centroid. Contour map of the layers (D_2) and (D_3) spectral depth values were obtained .

It is seen from the produced contour and maps of the Second layer (D_2) that there exist shallow depths in the North-eastern region of the study area and around the North-western part of the study area (Figure 3.6) and it can also be observed from the Third layer (D_3) contour and surface map exist deep depth at the north-western part of the study area (Figure 3.8).

4.3   Curie Point Depth Analysis

The magnetic field observation made at or above the surface of the earth and the magnetisation at the top of the magnetic rocks of the crust are characterised by relatively short spatial wavelength, while the magnetic field from the magnetisation at the curie-point depth will be characterised by longer wavelength and lower amplitude magnetic anomalies (Bahhtacharyya and Leu 1975; Okubo *et al*., 1985)

The obtained basal depth of a magnetic source is assumed to be Curie point Depth.

Table 3 above also gives the curie-point depth estimated from equation 3.23. Subsequently, contour map of the curie-point depth and its corresponding 3-D Model were generated and showed in Figure 3.9 and 3.10 respectively. The estimated depth to curie-point in this area varies from 5.72 to 14.84 km with average of 8.285 km. Previous workers such as Connard *et*

al., (1983), Bahhtacharyya and Leu 1975; Okubo *et al., (*1985) has indicated that the curie –

point depth is mostly dependent on the geological setting of the area under consideration.

4.4   Geothermal Gradient and Heat Flow Analysis

The calculated geothermal gradient and heat flow for the study area varies between 20.215

and 52.447^{o}C/km for geothermal gradient and 36.388 and 94.405 mW/m^2 for Heat flow

respectively. Contour and surface maps were produced as shown in Figure 3.11 – 3.14

respectively for the area of study.

The area indicated undulating heat flow with the highest value (94.405mW/m^2) found in the

North-eastern region of the study area which also corresponds to the area with the highest

geothermal gradient and vice-versa.

The average heat flow in a thermally 'normal' continental region is about 60-100 mW/m^2.

Values greater than 80-100 mW/m^2 indicate anomalous geothermal conditions (Jessop *et al.,*

1976). But the study area shows values less than 100mW/m^2 therefore the north eastern region

may likely to have geothermal potential.

CHAPTER 5

5.0   Conclusion and Recommendation

5.1   Conclusion

Previous workers such as Connard *et al.,* (1983), Bhattacharyya and Leu (1975) and Okubo *et al.,* (1985) have indicated that the curie – point depth is mostly dependent on the geological setting of the area under consideration. Tanaka *et al.,* (1999) pointed out that the Curie point depths are about 10 km or less in volcanic and geothermal areas, 15 – 25 km on island arcs and ridges, deeper than 20 km in plateaus and over 30 km in trenches. Although the geologic and physiography complexities of an area constrain the method, certain correlations between the Curie point depths and heat flow data area apparent and the Curie point depths are consistent with the tectonic settings. Good agreement between the curie points depths derived from heat flow data and magnetic data suggest that the Curie point depth analysis is useful to estimate the regional thermal structure.

The Curie point depth analysis determined from Spectral analysis performance applies to aeromagnetic data is 8.28 km as an average for the studied area. The Geothermal gradient and Heat flow values calculated varies from 20.215 to 52.447°C/km and 36.388 to 94.405 mW/m^2 respectively. The area showed an undulating heat flow with the highest value (94.405mW/m^2) found in the North-eastern region of the study area corresponds to the area with the highest geothermal gradient and vice-versa. Therefore the north-eastern region where higher heat flow is observed may be said to have geothermal potential.

5.2　Recommendation

The geothermal analysis based on geothermal gradients indicated areas of high gradient values in the north-eastern part of the study area; this part is likely a geothermal source zone in the study area.

It is recommended that radiometric studies be carried out to confirm the heat source in the north-eastern region of the study area where heat flow was observed.

REFERENCES

Armstrong, R. L. (1991). The Persistent Myth of Crustal Growth: *Australian journal of Earth Sciences 38,* 613 – 630.

Bath, M. (1974). *Spectral Analysis in Geophysics*. Netherland Amsterdam: Elsevier Scientific Publishing (pp.563).

Bertrand, S. J., Moussine, A. Pouchkine., & Fabre, J. (1977). Geodynamics of Cratonic Sedimentary areas examples Saharien: *Bulletin Centres Recherches Exploration-Production Elf- Aquitaine*, 1, 217 – 231.

Bhattacharyya, B. K. (1966). Continuous Spectrum of the Magnetic Field Anomaly Due to Rectangular Prismatic Body. *Geophysics* 31, 97 - 121.

Bhattacharyya, B. K., & Leu, L. K. (1975). Analysis of Gravity and Magnetic Analysis due to Two Dimension Structure: *Geophysics* 40, 993 - 1013.

Boler, F. M. (1978). Aeromagnetic Measurement, Magnetic Source Depths and the Curie Point Isotherm in the Vale-Owyhea, Oregon, M.Sc. Thesis, Oregon State University, Corvallis. *Journal of Geophysics Research Solid Earth* (pp. 99).

Burger, R. H., Sheehan, A. F., & Jones, C. H. (2006). *Exploring the Shallow Subsurface*. New York & London: W.W Norton & Company.

Cooley, J. W., & Turkey, J. W. (1965). An Algorithm for the Machine Calculation of Complex Fourier series Mathematics of Computation. *Geophysics,* 19, 297 – 301

Coney, P. (2009). *Plate Tectonics*, United State: Microsoft Encarta Premium 2009. Redmond, W A Microsoft Corporation.

Connard, G. R. Couch & Gemperte, M. (1983). Magnetic Anomalies & Curie- Point Isotherm Depth in the Cascade Mountain of Central Oregon. *Geophysics,* 48, 376 – 390.

Dobrin, M. B. (1976). *Introduction to Geophysical Prospecting*, (3rd ed.). New York: McGraw-Hill book Company (pp. 630).

Ewa, K., & Krzysztof, S. (2010). Geothermal Exploration in Nigeria. University of Silesia, Faculty of Earth Sciences, Department of Fundamental Geology: Bedzinska 60, 41-200 Sosnowiec, Poland.

Falconer, J. D. (1911). The Geology and Geography of Northern Nigeria: Macmillan London *Geographical Journal,* 14, 481 - 504.

Finkl, C. W. (2000). *Geophysics*. United State: Microsoft Encarta Premium 2009. Redmond, W A Microsoft Corporation.

Grant, F. S & West, G. F (1965). Interpretation Theory in Applied Geophysics. McGraw-Hill Inc. D2 Book 2, pp86. Retrieved from www.crcnetbase.com/doi/pdf/10.1201/9781420032147.ch6

Hahn, A., Kind, E. G., & Mishra, D. C. (1976). Depth Estimation of Magnetic Sources by Means of Fourier Amplitude Spectra. *Geophysical Prospecting,* 24, 278 - 308.

Henderson, R. G & Zietz, I (1967). The Computation of Second Vertical Derivatives of Geomagnetic Fields. *Mining Geophysics*, II, 606 – 614.

Japanese International Cooperation Agency (1990). *The Study of Groundwater Development in Sokoto state of Nigeria*, Progress Report 3, 4 and 5. Nigeria.

Jessop, A. M. (1976). Heat flow Anomalies from the Spectral Analysis of Airborne Magnetic Data of Nupe Basin, Nigeria. *Asian Journal of Earth Sciences*, 4, 20 - 28

Kangkolo, R. (1996). A Detailed Interpretation of the Aeromagnetic Field over the Mamfe Basin of Nigeria and Cameroon, Ph.D. thesis, Ahmadu Bello University Zaria, Nigeria.

Kogbe, C. A. (1979). Geology of South Eastern Sokoto sector of the Iullemmenden Basin. Bulletin Department of Geology, Ahmadu Bello University Zaria, Nigeria (pp.420).

Naidu, P. S. (1970). Statistical Structure of Aeromagnetic fields, *Geophysics, 35(2),* 279 - 292.

Negi, J. G. Agrawai, P. K & Rao, K. N. (1983). Three Dimensional Model of the Koyna Area of Maharashtra State (India) Based on the Spectral of Aeromagnetic Data. *Geophysics, 48(7),* 964 - 974.

Nemzer., Marilyn, L., Carter, A., & Kenneth Press (2009). *Geothermal Energy.* United State: Microsoft Encarta Premium 2009. Kenneth press.

Oppenheim, A. V., & Schafer, R. W. (1975). *Digital Signal Processing Practice*. New Jersey hall International Company (pp.585).

Patchett, P. J., & Samson, S. D (2003). Ages and Growth of the Continental Crust From Radiogenic Isotopes the Crust, (Ed. Rudnick 3:321-348 of treatise of Elsevier Perganon Oxford)

Pal, P. C., Khurana, K. K., & Unnikrishnan, P. (1978). Two examples of Spectral Approach to Source Depth Estimation in Gravity and Magnetic, 117, 772 - 783.

Raeburn, C., & Tattam, C. M. (1930). A Preliminary Note on Sedimentary Rocks of Sokoto Province, *Bulletin Geology Survey of Nigeria* 13, 57 - 60.

Reiter, M. A., & Jessop, A. M. (1985). Estimates of Terrestrial Heat Flow in offshore Eastern Canada, *Canadian Journal of Earth Science* 22, 1503 - 1517.

Salem, A. K., Elsirafi, A., & Mizanage, H. (2000). Spectral Analysis of Aeromagnetic Data for Geothermal Reconnaissance of Quseir Area Northern Red sea Egypt: Proceedings of the World Geothermal Congress (WGCOO) Kyushu, *Journal of Mining Geology and Geological Society*, 1, 1669 - 1673.

Sharma, P. V. (1987). Magnetic Methods Applied to Mineral Exploration: Ore Geology Reviews 2, 323 - 357.

Shehu, A. T. (2004). Spectral Analysis of the magnetic Residual Anomalies over the Upper Sokoto basin Nigeria, Unpublished M.Tech Thesis, Federal University of Technology, Minna. Niger State

Spector, A. & Grant, F. S. (1970). Statistical Models for Interpreting Aeromagnetic Data, *Geophysics* 35, 293 – 302.

Stacey, F.D (1977). Basement Curie Isotherm and Shallow Crustal Structure of the Trans-Mexican Volcanic Belt from Aeromagnetic Data, *Tectonophysics, 172(1),* 77 - 90.

Tanaka, A., Okubo, Y., & Matsubayashi (1999). Curie point Depth Based on Spectrum Analysis of the Magnetic Anomaly Data in East and Southeast Asia, *Tectonic Physics* 306, 461- 470.

Telford, W. M, Geldart, L. P, Sheriff, R. E & Keys, D. A (1976). Applied Geophysics, *Cambridge University Press.* (pp. 860).

Treital, W.G., Clement, & Kaul, R. K. (1971). The Spectral Determination of Depth to Buried Magnetic Basement Rocks. *Geophysics Journal of the Royal Astronomical Society* 24, 415 – 428

Turcotte, D. L., & Shubert, G., Stampolidis, N. C (1982). Curie point Depth from Spectral Analysis of Magnetic Data in Erciyes Stratovolcano, (Central Turkey) 167 (2010). Curie point Depth of the Erciyes Region 353. *Pure and Applied Geophysics* 159, 1 - 13

Udensi, E. E., Shehu, A. T., Adeniyi, J. O., & Jonah, S. A. (2004). Spectral Analysis of the Magnetic Residual Anomalies over Upper Sokoto Basin Nigeria. *Zuma Journal of Pure and Applied science,* 6(2), 37- 49.

Umego, M. N. (1990). Structural interpretation of Gravity and aeromagnetic Anomalies over Sokoto Basin North-western Nigeria. Unpublished PhD Thesis Ahmadu Bello University, Zaria Nigeria.

APPENDIX